AD-A269 926

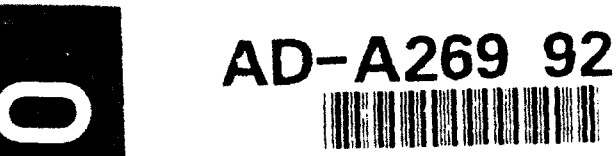

CRREL

DTIC
SEP 29 1993

DISTRIBUTION STATEMENT A
Approved for public release;
Distribution Unlimited

CRREL REPORT 93-10

Thermal Stress Measurements in Asphalt Concrete

Vincent Janoo, John Bayer Jr. and Michael Walsh

July 1993

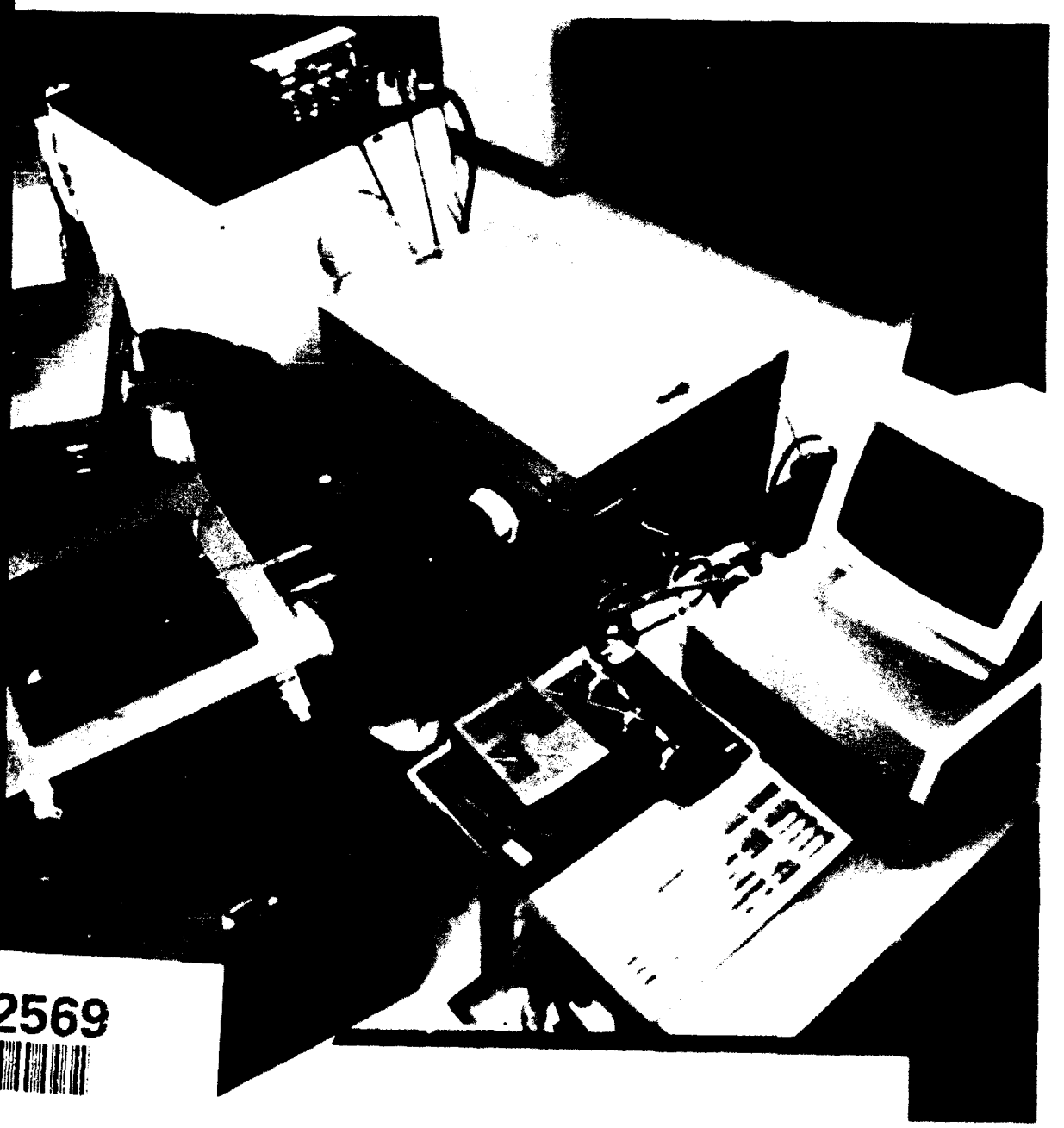

93-22569

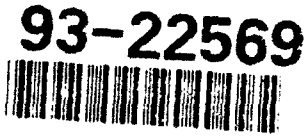

Abstract

Asphalt concrete (AC) pavements in cold regions are prone to thermal cracking. There are two theories to explain this. The first one is that at some low temperature, the thermal stress in the pavement structure exceeds the tensile strength of the mixture, usually in the winter. The second is that the AC mixture fails through thermal fatigue that is caused by daily temperature cycling. There are many ways of characterizing AC performance at low temperatures, and this report summarizes the different failure criteria and test methods for doing this. One test method described here that CRREL has developed is a thermal stress test device for measuring thermally-induced stresses in the laboratory. The device can be used for monotonic and cyclic loading, while various temperature drop rates can be applied to the specimen. The calibration of the test apparatus, loading pattern and specimen configuration used are described and typical results are presented.

Cover: Step-motor system.

For conversion of SI metric units to U.S./British customary units of measurement consult *Standard Practice for Use of the International System of Units (SI)*, ASTM Standard E380-89a, published by the American Society for Testing and Materials, 1916 Race St., Philadelphia, Pa. 19103.

CRREL Report 93-10

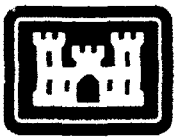

US Army Corps of Engineers
Cold Regions Research & Engineering Laboratory

Thermal Stress Measurements in Asphalt Concrete

Vincent Janoo, John Bayer Jr. and Michael Walsh

July 1993

Prepared for
OFFICE OF THE CHIEF OF ENGINEERS
and
U.S. DEPARTMENT OF TRANSPORTATION
FEDERAL AVIATION ADMINISTRATION

Approved for public release; distribution is unlimited.

PREFACE

This report was prepared by Dr. Vincent C. Janoo, Research Civil Engineer, and John J. Bayer, Jr., Engineering Technician, both of the Civil and Geotechnical Engineering Research Branch, Experimental Engineering Division, and Michael R. Walsh, Mechanical Engineer, Engineering Resources Branch, Technical Resources Center, U.S. Army Cold Regions Research and Engineering Laboratory. Funding was provided by the U.S. Department of Transportation, Federal Aviation Administration, under Interagency Agreement DTFA01-89-Z-02050, and the Office of the Chief of Engineers through DA Project 4A762784AT42, *Design, Construction and Operations Technology for Cold Regions*, Task BS, Work Unit 003, *Asphalt Pavements in Cold Regions*.

The authors thank E. Chamberlain (CRREL) and H. Tomita (FAA) for technically reviewing this report. Appreciation is also expressed to D. Garfield, F. Gernhard and his machine shop crew, T. Tantillo, R. Farr, K. Rezendes and F. Carver for their assistance in developing the test equipment and writing the report. Special thanks go to M. Hardenberg for editing this report and E. Perkins and M. Pacillo for drafting the figures.

The contents of this report are not to be used for advertising or promotional purposes. Citation of brand names does not constitute an official endorsement or approval of the use of such commercial products.

Accession For	
NTIS GRA&I	☑
DTIC TAB	☐
Unannounced	☐
Justification	
By	
Distribution/	
Availability Codes	
Dist	Avail and/or Special
A-1	

DTIC QUALITY INSPECTED

CONTENTS

ILLUSTRATIONS

Figure

TABLES

Thermal Stress Measurements in Asphalt Concrete

VINCENT JANOO, JOHN BAYER JR. AND MICHAEL WALSH

INTRODUCTION

Thermal cracking in Asphalt Concrete (AC) pavements is a serious problem in the U.S., Canada, Japan and parts of Europe. It has been reported in the continental U.S. at locations where the air freezing index is as little as 361°C day (Fig. 1). (Finn et al. 1976). Thermal cracks usually run transversely across road and airfield pavements (Fig. 2). Such cracks in pavement structures are a problem because they act as conduits for the migration of water and fines into and out of the pavement, which, depending on the drainage conditions in the pavement structure, can cause a saturated condition in the base, subbase and subgrade. If this happens, it is possible that when truck or aircraft wheel loads are applied to the saturated pavement structure, there will be excessive pore water pres-

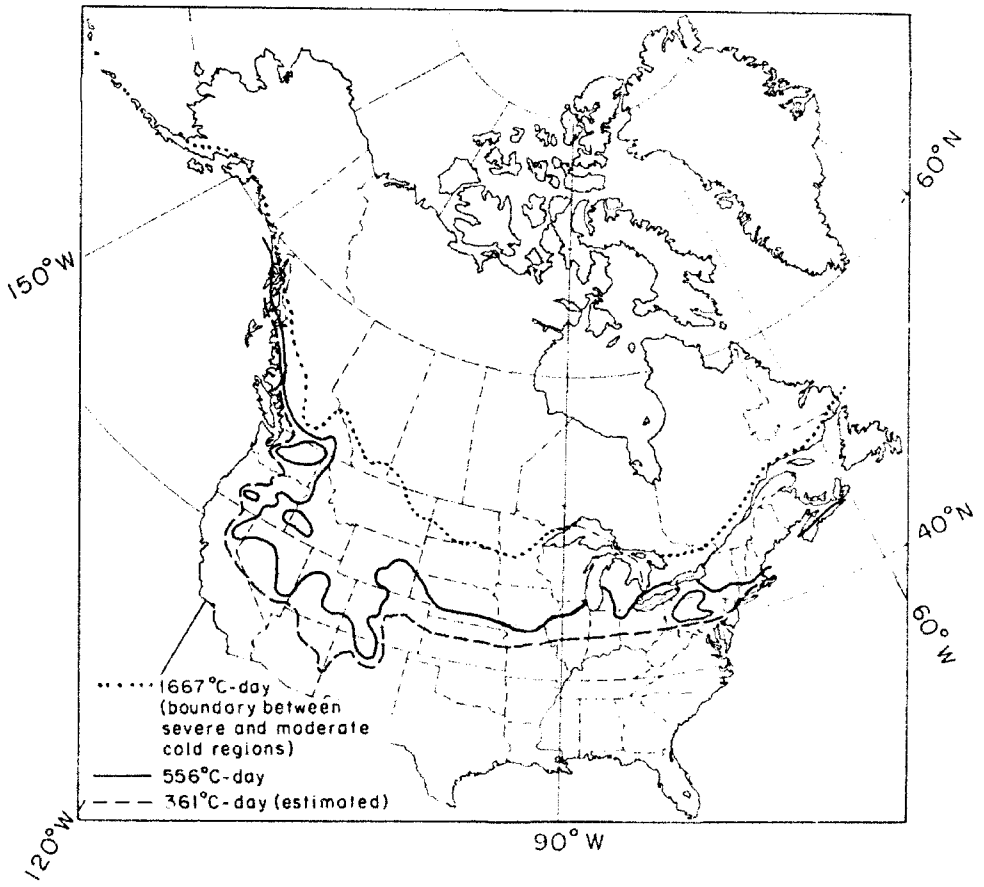

Figure 1. Above the 361°C-days line is the area of temperature cracking in North America.

a. Typical transverse cracks.

b. Localized failure around a transverse crack.

Figure 2. Thermal cracks.

sures in the underlying layers, thus reducing the effective bearing capacity of the unbound base and the upper subgrade layers. Transient wheel loads can also cause pumping of fines through these cracks, which can produce voids under the pavement. Additional stress cracking around the initial thermal crack (Fig. 2b) will be the result.

The economic impact of thermal cracking has been reported in the literature. For example, Haas et al. (1987) reported that the Canadian Air Transport Administration could have saved approximately $10 million (1985 Canadian dollars) in maintenance costs if thermal cracking was reduced by 50% only. Linde (1988) cited a 1972 U.S. Air Force report that estimated damage to airplanes caused by pavement cracking was about

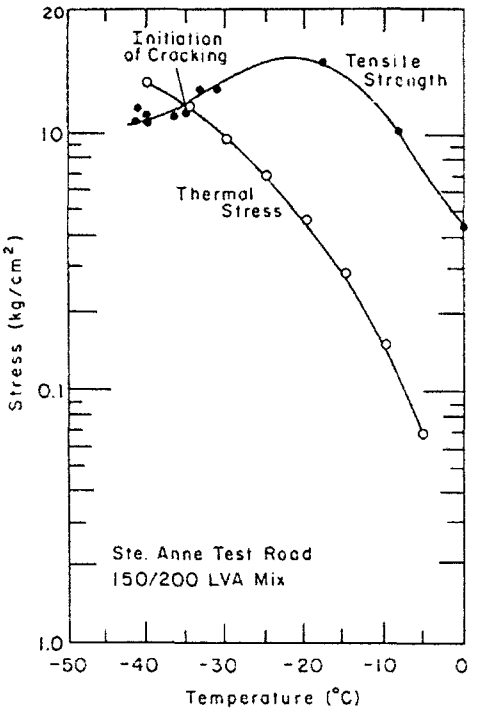

Figure 3. Prediction of fracture temperature for a restrained strip of asphalt concrete.

$130 million annually. Another economic benefit of reducing thermal cracking is extending the time before sealing or an overlay is required.

Currently, there are two theories on why thermal cracks occur. The first states that thermal cracking happens when the thermal stress (from low temperatures) in the AC pavement exceeds the tensile strength of the AC mixture. This is called *low-temperature cracking;* it is associated with the volumetric contraction that takes place in a material as the temperature drops. If the material is restrained, as in the case of a competent, new AC layer in a pavement structure, the tendency to shorten results in a thermal stress that produces cracking when it exceeds the tensile strength of the material. Figure 3 shows this situation. The temperature at which the pavement fails is called the fracture temperature. In fairly new pavements, cracks generally have been observed to appear at a spacing of 30 m or more. But, as the pavement ages or there are greater temperature drops, the crack spacing can decrease to 3–6 m.

Observing transverse cracks in Texas caused Shahin and McCullough (1972) to propose a second theory for thermal cracking. The extreme low temperatures required for low-temperature cracking are rarely found in Texas (McLeod 1970). Shahin and McCullough suggested that thermal cracks can also occur when AC pavements are subjected to temperature cycling from the daily daytime high and nighttime low temperatures, causing what they call *thermal fatigue*, a concept similar to load-induced fatigue.

It is clear from past research that the stiffness of the asphalt cement has a strong influence on thermal cracking. There are several factors, however, other than the properties of the asphalt cement that influence the initiation and frequency of thermal cracking. These are aggregate type, type of subgrade, traffic and even pavement thickness (Deme and Young 1987, Janoo and Chamberlain 1987, Janoo et al. 1990). The current emphasis, though, is to relate asphalt cement properties and indices, such as viscosity and penetration, to low-temperature performance of AC pavements in cold regions. The viscosity or penetration values, or both, are used to produce one of two temperature susceptibility indices: the Penetration Index (PI) and the Penetration Viscosity Number (PVN). They are used extensively to characterize the performance of AC at low temperatures. There are, however, several drawbacks to using these indices. First, the indices depend on either the petroleum refining technique or on the amount of wax present in the asphalt. Second, these indices are developed from tests conducted at temperatures of 4, 25 and 135°C, making it necessary to extrapolate from the measured data to estimate the asphalt properties at low temperatures.

CRREL, in conjunction with the Federal Aviation Administration (FAA), is conducting research on characterizing the performance of AC pavements in cold regions. Part of this research is characterizing the engineering properties of AC mixtures at low temperatures, which we divided into three parts. First, we conducted a field study of the performance of "soft grade" AC mixtures in cold climates (Janoo 1990). Second, we developed a laboratory test method for characterizing *asphalt mixture* properties at low temperatures. The test method required the development of equipment for measuring thermally induced loads in an asphalt mixture subjected to low temperatures in the laboratory. Finally, we initiated a test program to study the engineering properties of unmodified and modified AC mixtures at low temperatures. The third stage of the research has been started but not completed. This report summarizes the results of the second phase, i.e., the development of a testing apparatus for measuring the thermal loads in an AC mixture. The report starts with a brief summary of current prediction models and test

methods for predicting low-temperature performance of AC. Then the development of the CRREL Thermal Stress Test (CTST) equipment is outlined. Finally, some of the test results from the CTST are presented.

PREDICTION OF LOW-TEMPERATURE CRACKING

There are several models for predicting low-temperature cracking, such as the viscous-flow-temperature method (Fromm and Phang 1972) and the penetration (PI) method (Sugawara et al. 1982), but the two most commonly cited in the literature are:

1. The mix cracking temperature method.
2. The limiting mix stiffness method.

Using the properties of the AC *mixtures*, the methods try to predict the *fracture temperature* at which cracks are initiated in the AC pavement. Failure in either method is reported as the temperature at which the cracking starts.

Mix cracking temperature method

This model's failure criterion is that the pavement will fracture when the thermally induced stresses exceed the tensile strength of the AC mixture. Computer programs such as COLD (Finn et al. 1986) and TC-1 (Shahin and McCullough 1972) use this failure criterion for predicting low-temperature cracking.

The thermal stress in the AC is calculated using analytical methods. For example, Monismith et al. (1965) used the stress equations developed by Humpreys and Martin (1963) to predict the stresses in a slab of a linear visco-elastic material subjected to a time-dependent temperature field. Based on results from the Ste. Anne test road, Christison et al. (1972) found that, in representing the AC layer as a visco-elastic slab, their analysis tended to overestimate the thermal stresses in the slab. If they modeled it as a visco-elastic beam, the thermal stresses were underestimated, and modeling the AC as a pseudo-elastic beam yielded intermediate values. In the end, for the sake of simplicity, COLD and TC-1 calculate the thermal stresses using the pseudo-elastic equation of Hills and Brien (1966). The equation is

$$\sigma_x(t) = \int_{t_0}^{t} \alpha(T)\, S(t,T)\, dT(t) \qquad (1)$$

where $\sigma_x(t)$ = accumulated thermal stress
$\alpha(T)$ = coefficient of thermal contraction
$S(t,T)$ = asphalt mix stiffness, function of time and temperature
$dT(t)$ = temperature drop (cooling rate).

The material properties required in eq 1 are the coefficient of thermal contraction and the stiffness of the AC. It can be solved numerically using the finite difference method. If the coefficient of thermal contraction (α) is independent of temperature, eq 1 can be approximated as

$$\Delta(\sigma x)_i = \frac{\alpha}{2}(S_i + S_{i-1})(T_i - T_{i-1}). \qquad (2)$$

Hills and Brien (1966) and Christison et al. (1972) used a loading time (t) equal to the time step ($t_i - t_{i-1}$) to calculate the stiffness of the AC.

One of the drawbacks with the pseudo-elastic method is that the stresses calculated from eq 1 are dependent on the time interval (t) used in the numerical evaluation (Christison et al. 1972). Modeling the AC as a visco-elastic material eliminates this time step dependency, but it requires a greater computational effort than the pseudo-elastic analysis (Christison et al. 1972). With the availability of high-powered personal computers, the effort required for the analysis can be reduced easily. Better characterization of the visco-elastic properties of AC will produce better estimates of the thermal stress.

As mentioned above, one of the material properties required in eq 1 is the coefficient of thermal expansion (contraction). Monismith et al. (1965), Littlefield (1967), Jones et al. (1968) and Osterkamp et al. (1986) reported measurements on thermal shrinkage of asphalt pavement. Several methods were cited in the literature for measuring the thermal expansion: strain gages, dual microscope apparatus, LVDTs, and water- and mercury-filled dilatometers. From these measurements the coefficient of thermal contraction is back-calculated. This material property is usually held constant in

Table 1. Coefficient of thermal contraction (α) of AC mixtures.

Investigators	$\alpha \times 10^{-6}$ *(1/°C)*	*Temperature range (°C)*
Monismith et al. (1965)	2.2–2.5	–23 to 21
Jones et al. (1968)	2.0	–37 to 16
Burgess et al. (1971)	1.7–2.2	–40 to 20
Osterkamp et al. (1986)	1.7–2.2	–56 to 6.4
Sugawara et al. (1982)	2.0	?
Sato et al. (1982)	2.1–3.0	–20 to 10
This study	2.4	–40 to 0

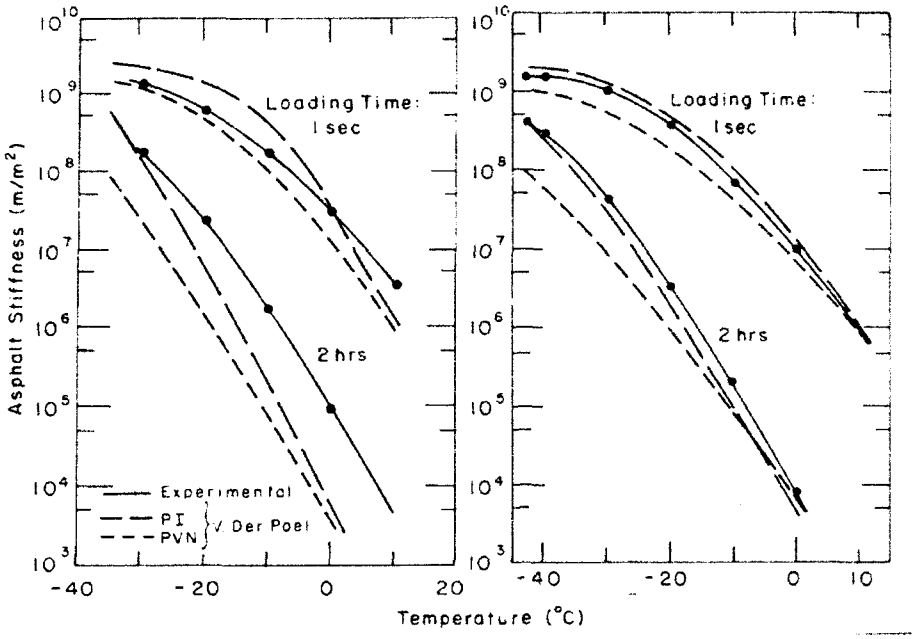

Figure 4. Comparison of calculated and measured asphalt stiffnesses—high wax on the left, low wax on the right (after Gaw 1978).

the analysis. Typical values reported are presented in Table 1.

The second material property required in eq 1 is the stiffness of the AC mixture. It is generally estimated by first estimating the asphalt cement stiffness using Van der Poel's (1954) nomograph. The stiffness of the asphalt cement is then used with either the Heukelom and Klomp (1964) relationship between asphalt and mixture stiffness or the Bonnaure et al. (1977) nomograph to estimate the AC stiffness. Gaw (1978) compared measured and calculated asphalt cement stiffness and found significant differences in the asphalt stiffness values at low temperatures (Fig. 4). The differences were attributable to the type of asphalt and the temperature susceptibility index (PI or PVN) used. The data also showed that loading time greatly affected both the calculated or measured stiffness.

The calculated thermal stress from eq 1 is then compared with the tensile strength of the AC mixture, which can be determined from indirect or direct tension tests. The indirect tension test, also called the tensile splitting test, has been used extensively to characterize the stress–strain response of AC at low temperature (Shields 1964, Christison 1966, Anderson and Hahn 1968, Haas and Anderson 1969, Shields et al. 1970, Christianson 1970, Dempsey et al. 1980, Anderson and Epps 1983, Anderson and Leung 1987, Hadipour and Anderson 1988). The test consists of loading Marshall specimens (102 mm in diameter and 64 mm thick)

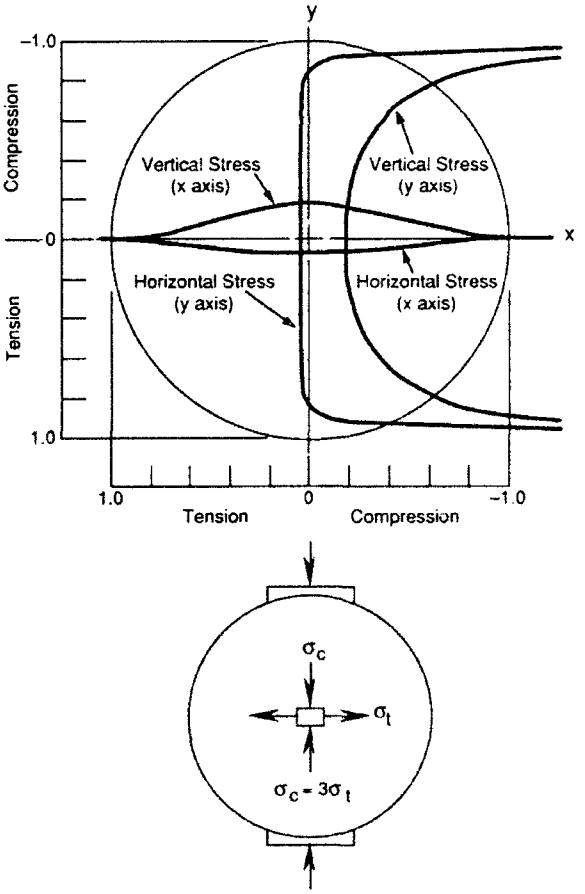

Figure 5. Relative stress distributions and element showing biaxial state of stress for the indirect tensile test (after Kennedy 1977).

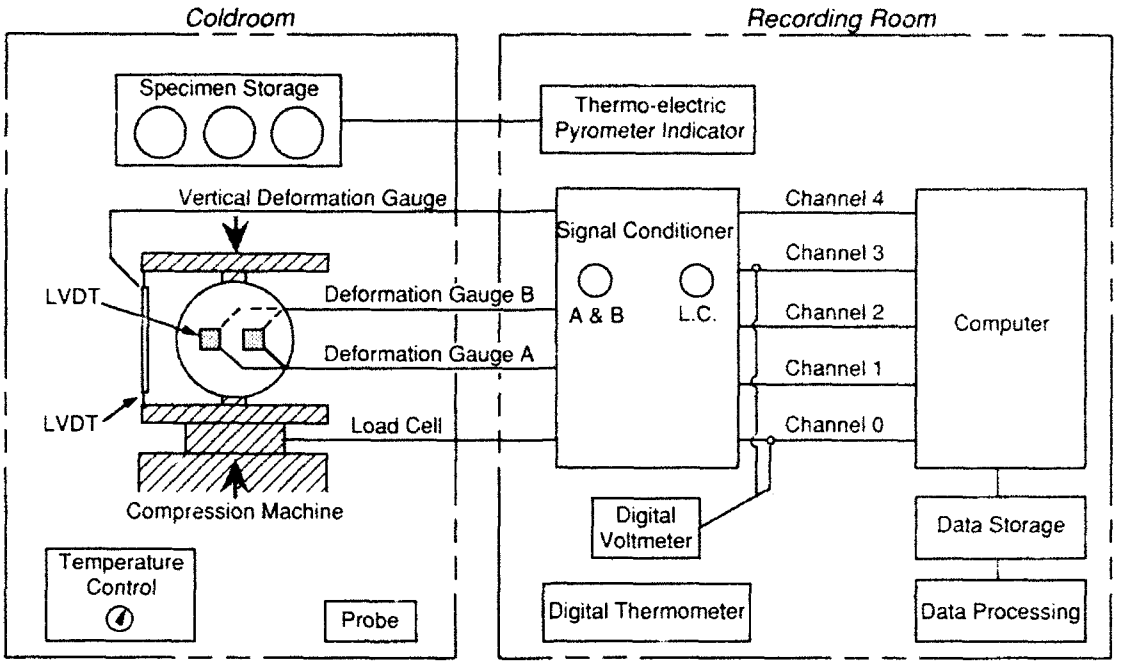

Figure 6. Diametrical indirect tension test equipment.

across a diameter in a compression testing frame. As the specimen is compressed at a set temperature and load application rate, a relatively uniform tensile stress develops on the vertical diametrical plane of the specimen (Fig. 5). Ultimately, the specimen is subjected to a failure load and it fails by splitting along its vertical diameter. The applied load, and horizontal and vertical deformations are monitored with a load cell and LVDTs respectively. A schematic of the tensile splitting test is shown in Figure 6.

The theoretical basis of the tensile splitting test is the theory of elasticity and the assumption of a plane stress condition ($\sigma_z = 0$). As the specimen is loaded, a biaxial stress state develops in it (Fig. 5). Besides the tensile stress on the vertical plane, compressive stresses are generated on the vertical and horizontal planes. The compressive stresses on the vertical plane (y-axis) can be greatly reduced (but not eliminated) when the point load is substituted with a distributed load via a loading strip. The tensile stress at the center is given by

$$\sigma_t = \frac{-2P}{\pi d t}$$

where σ_t = tensile stress
P = applied load
d = diameter of specimen
t = thickness of specimen.

A more rigorous method for calculating the tensile strength from the indirect tension test can be found in Kennedy (1977).

The tensile strength obtained from this test depends on the loading rate (Fig. 7). It appears from the data that, below -10°C, the effect of loading rates is insignificant, while above 0°C the effect is significant. The higher the loading rate is, the higher is the tensile strength. Several loading rates have been cited in the literature for simulating thermal loading: Anderson and Leung (1987) used a loading rate of 1.5 mm/min; Von Quintus et al. (1988) used a loading rate of 1.25 mm/min; and Dempsey et al. (1980) used a loading rate of 1.8 mm/min.

The effect of temperature on the tensile strength of AC is shown in Figure 8, with the exception of cold lake asphalt. The softer grade—200/300 pen—asphalt mixture (Fig. 8b) reaches its peak tensile strength at much lower temperatures than the harder 85/100 pen asphalt, which reaches its peak strength at around -10°C.

In general, the indirect tension test is popular because of its simplicity. It requires the common Marshall test specimens and it has been used extensively over the years. However, as Haas (1973) pointed out, the stress state in a specimen subjected to an indirect tensile test is more complex than what is assumed in the calculations of tensile stress. The total deformation measured (hence the

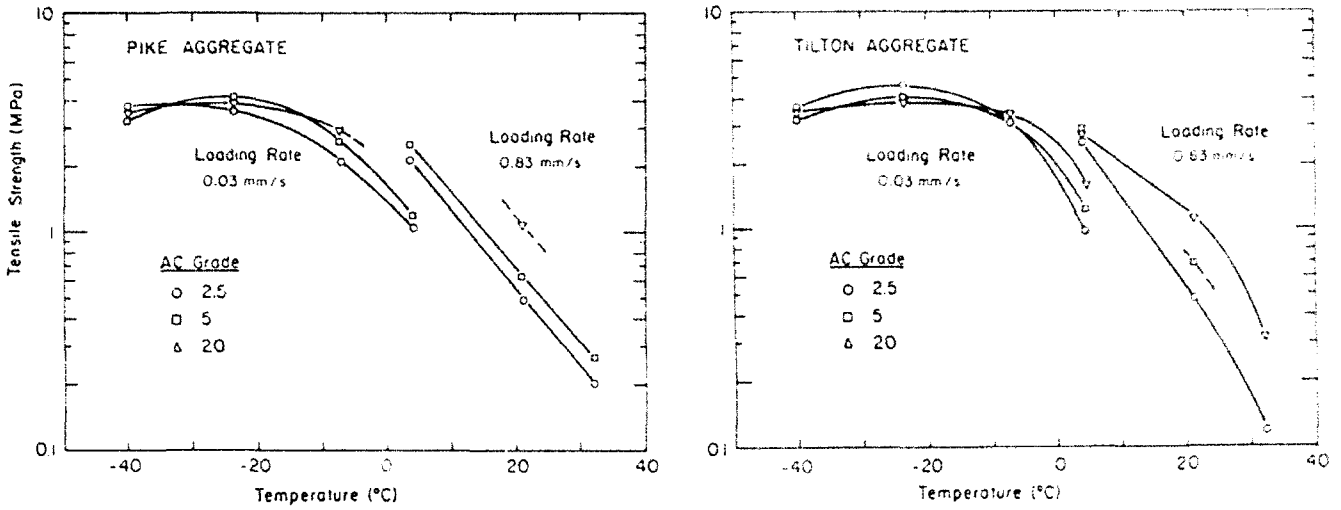

Figure 7. Effects of asphalt grades, rate of loading and temperature on indirect tensile strength (75-blow compaction) (after Dempsey et al. 1980).

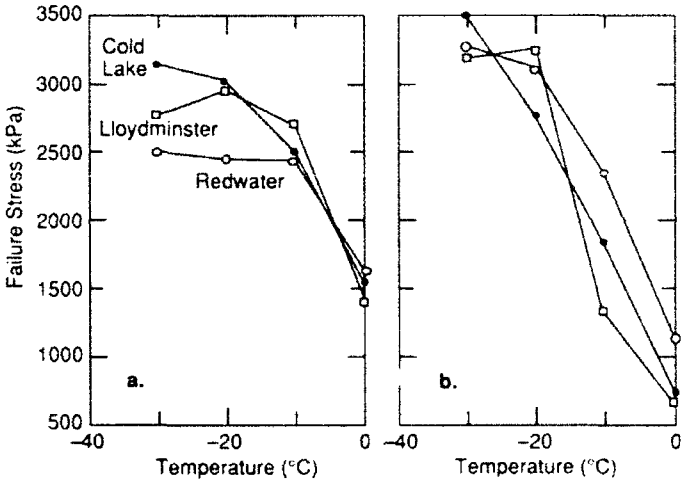

a. 85/100 Pen. *b. 200/300 Pen.*

Figure 8. Failure stress–temperature relationship (after Haas 1973).

strain calculated) is the resultant of the compression and tensile deformation in the specimen. With respect to thermal cracking, the loading condition used and the mode of fracture do not simulate actual field conditions. The results of this test therefore do not characterize the actual low-temperature response of AC. At best, it is an index for characterizing low-temperature performance.

Haas (1973) developed the direct tension test for determining the tensile strength of AC at low temperatures. This test was basically developed to overcome some of the problems of the indirect tensile test. He used a rectangular AC beam that was 38 mm square × 102 mm long, and subjected it to a uniaxial tensile load at a set temperature and rate of extension. A schematic of the test system is shown in Figure 9. Haas (1973) suggested that, concerning low-temperature behavior, this test more closely simulates the actual stress state and fracture mode. Since low-temperature shrinkage fracture occurs under a slow buildup of tensile stresses, the rate of extensions used in the test are very low. Haas' (1973) guidelines for rates of extension to be used are from 2.4 to 12 cm/s as the temperature increases from –30 to 30°C. Kallas (1982) conducted similar tests and used an extension rate of 8.3×10^{-4} cm/s at low temperatures. The measured parameters from this test are load, extension of the specimen, test temperature and time to failure. Typical stress–strain curves from this test method are shown in Figure 10.

The direct tension test described above has not

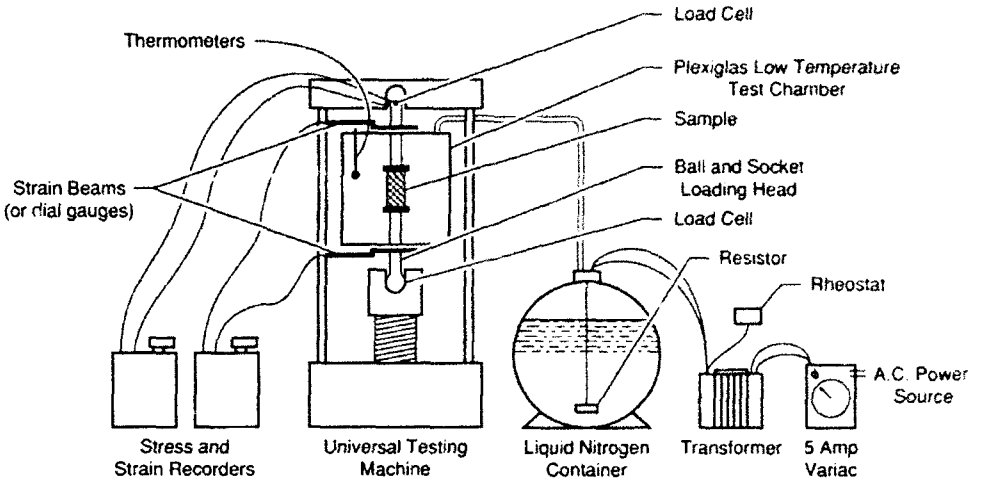

Figure 9. Direct tension and creep load test system (after Haas 1973).

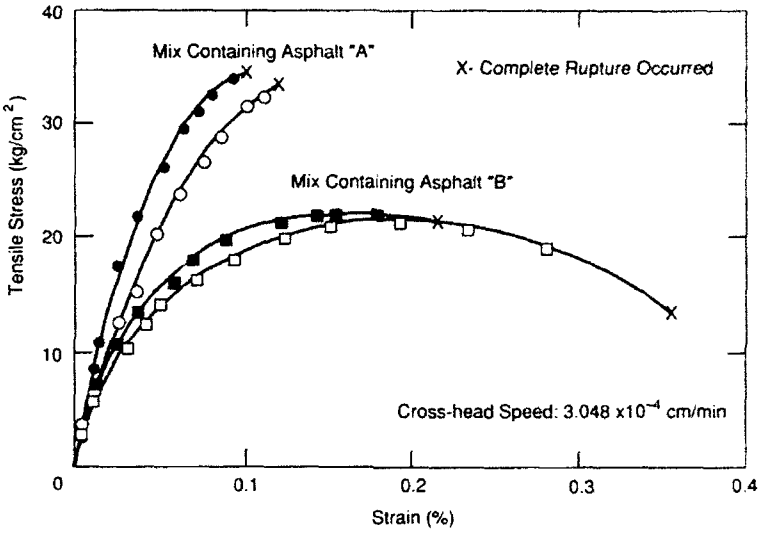

Figure 10. Stress–strain curves at temperature of –18°C from constant rate extension tests (after Haas 1973).

been as popular as the tensile splitting test. It is slightly more complex to run, and special test specimens need to be fabricated. Most of the experience with this test method comes from the University of Waterloo, the Asphalt Institute and the Ontario Ministry of Transportation; however, as mentioned above, this test does come closer to simulating field conditions. A drawback to this test is the specimen size. For example, for a mix containing aggregates having a maximum diameter of 19 mm, the minimum cross-sectional area of the test specimen is 45 cm^2 (under the assumption that, for the specimen to be homogenous, the minimum-diameter-to-grain-size ratio is 4).

We have tested 76-mm-square specimens. We were able to restrict the failure planes to the middle third of the specimen if we kept the specimen-length-to-width ratio to 2.5. Increasing the ratio produced failures close to the ends. We suspect that the fracture strength obtained from the smaller test specimens may be higher than what they really are. Another drawback is that, as for the indirect tension test, the rate of cooling is simulated by an arbitrary rate of extension.

Limiting mix stiffness method

This method's failure criterion is that the pavement will crack when the AC mixture reaches a limiting stiffness value. McLeod's (1970) experience with pavements in Canada and the northern U.S. led him to conclude that pavements cracked when the mix stiffness reached 6.9×10^9 N/m^2 at a loading time of 20,000 seconds. Gaw et al. (1974), on the basis of results from the Ste. Anne test road, concluded that cracking occurred when the mix stiffness reached 18×10^9 N/m^2 at a loading time

of 1800 seconds. Carpenter and VanDam (1985) suggested that cracking would take place when the stiffness of the mix reached 3.5×10^9 N/m^2 at a loading time of 20,000 seconds. Readshaw's (1972) study of thermal cracking in British Columbia determined that cracking happened when the stiffness of the mix reached 2×10^8 N/m^2 at a loading time of 7200 seconds.

Because the mix stiffness is a function of temperature, asphalt grade, asphalt content and air voids, it is doubtful if any one value of limiting mix stiffness can be used for predicting the onset of thermal cracking. However, an Ad Hoc Committee of the Asphalt Institute (1981) has recommended a stiffness value of 18×10^9 N/m^2 as a reasonable limiting stiffness value. But, they recommended that more experimental stiffness data, correlated with observed pavement cracking temperatures, be obtained in a way similar to that used on the Ste. Anne test road (Gaw et al. 1974).

The limiting mix stiffness can be estimated using the asphalt stiffness and Huekelom and Klomps' (1964) relationship between asphalt and mix stiffness or the nomograph of Bonnaure et al. (1977). In addition to the above, the stiffness can also be obtained from creep and flexural bending tests.

From the indirect tension test, the stiffness modulus can be calculated (Anderson and Leung 1987) from

$$S_t = \frac{0.912\sigma_t}{0.5\varepsilon_{avg}}$$

where S_t = tensile stiffness modulus (MPa)
σ_t = tensile stress (MPa)
ε = average tensile strain (mm/mm).

The stiffness of an AC mix can also be calculated from direct tension and creep tests (Fromm and Phang 1972, Hass 1973). From the direct tension test, the stiffness at any time at a set temperature is calculated from

$$S_t = \frac{\sigma_t}{\varepsilon}.$$

The tensile creep test can also be used to determine the stiffness of the AC. This test is conducted by applying a constant load to a specimen maintained at a constant temperature. A typical recording of the resulting deformation with time is shown in Figure 11.

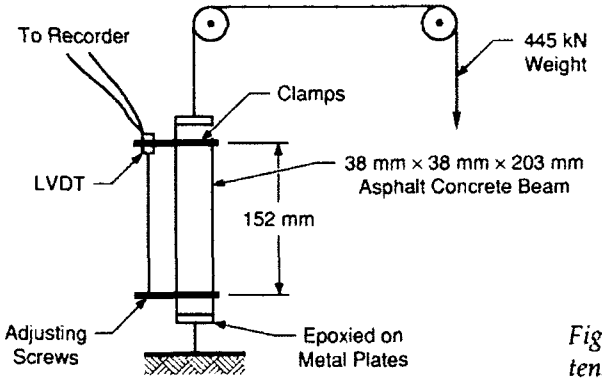

a. Measurement device.

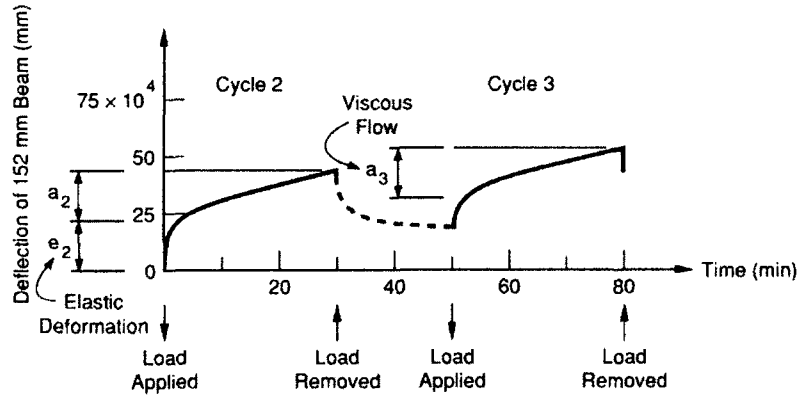

b. Results.

Figure 11. Measurement of creep deformation under constant tensile stress (after Fromm and Phang 1972).

Table 2. Some examples of creep loads (after Haas 1973).

Temperature (°C)	Cross-sectional area (mm^2)	Load level for time of loading (>2 hr) (kg)
-34	1452	227
-18	1452	249
-1	1452	68

Specimen sizes have varied in creep tests. Haas (1973) used a 38- × 38- × 102-mm specimen. Fromm and Phang (1972) used a test specimen with a similar cross section but longer (203-mm). Results of creep tests conducted at temperatures as low as –23°C have been reported in the literature (Fromm and Phang 1972). The applied loads are not constant, as higher loads are required at lower temperatures. For the 14.4-cm^2 cross-sectional area, Hass (1973) provided some guidance for the load level that could be used in low-temperature creep tests (Table 2). Fromm and Phang (1972) used a 30-minutes-on, 20-minutes-off load cycle for their creep tests, measuring the load, deformation, temperature and time. A typical load deformation curve from a creep test is shown in Figure 11.

The stiffness of the mix at a given time and temperature is calculated from

$$S_{ct} = \frac{\sigma_0}{\varepsilon}.$$

where σ_0 is the applied load. Hass (1973) showed that the stiffnesses obtained from the creep test or the direct tension test were similar to each other (Fig. 12). The stiffnesses calculated from these tests were much lower than those predicted by either the Heukelom or McLeod estimation methods.

As with the direct tension test, the major drawbacks to tensile creep tests are the small cross-sectional areas of specimens used and the simulation of thermal loading by mechanical means. However, both tests are a step forward when compared to the indirect tension test.

The stiffness modulus of AC has been determined from the flexural bending test (Rader 1935, 1937; Busby and Rader 1972; Sugawara et al. 1982). Busby and Rader (1972) used 89-mm-wide × 83-mm-deep × 381-mm-long test specimens in a three-point loading test. Sugawara et al. (1982) used 25- × 25- × 250-mm test specimens. To simulate thermal loading, Busby and Rader (1972) used a slow rate of loading of 0.5 mm/min. For smaller beams (51-mm width × 38-mm depth × 152-mm length), Rader (1935) used a loading rate of 1.3 mm/min. Sugawara et al. (1982) used strain rates of 10^{-4} to 1.9/s at test temperatures ranging from –37 to 30°C.

The stiffness modulus is determined from

$$S_t = \frac{dPL^3}{48\delta I}$$

where dP = change in load
L = span of beam
δ = corresponding deflection due to dP
I = moment of inertia.

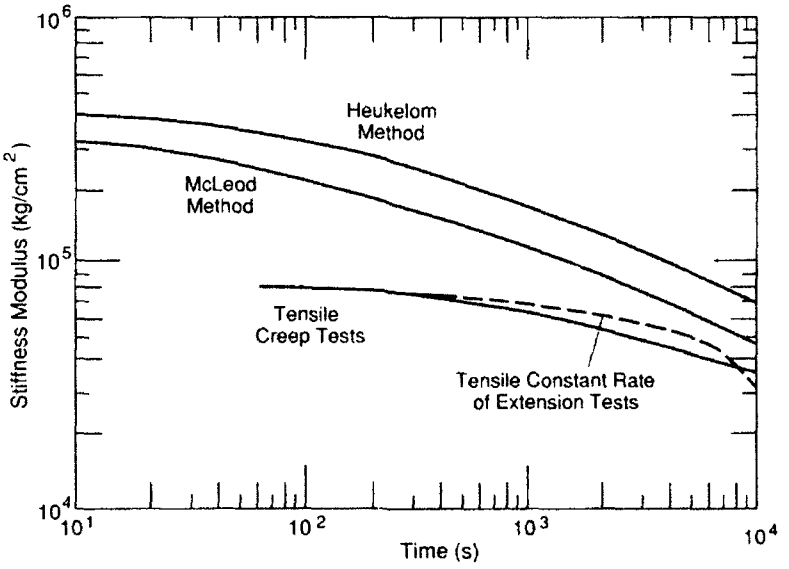

Figure 12. Relationship between stiffness modulus and time (after Haas 1973).

The maximum stress, i.e., the tensile strength of the AC mixture, can be calculated from

$$\sigma_t = \frac{PLc}{2I}$$

where σ_t = tensile strength
P = failure load
c = one-half depth of beam.

DIRECT MEASUREMENTS OF FAILURE STRESS AND TEMPERATURE

Attempts to measure the thermally induced loads in AC started in earnest in the mid-1960s. The direct measurement of low-temperature failure stresses and temperatures has been reported by Monismith et al. (1965), Hills and Brien (1966), Tuckett et al. (1970), Chipperfield and Fabb (1971), Fabb (1974), Sugawara et al. (1982), Sugawara and Moriyoshi (1984) and Arand (1987). Currently, as part of the research project to characterize mixtures, the Strategic Highway Research Program (SHRP), under the 003-A contract, has developed equipment for measuring the thermally induced load in a restrained AC specimen. CRREL was a consultant to SHRP in the development of the test equipment.

In general, the test attempts to restrain an AC specimen and measure the thermally induced tensile loads as the temperature drops. Basically, the ends of an AC test specimen are fixed by a rigid frame, and a load cell is attached between the specimen and the rigid frame. The specimen, or in some cases the whole experimental setup, is placed in an environmental chamber, where the temperature is then dropped and the load cell monitored. As the temperature drops, the specimen tries to shrink. But, since it is restrained by the rigid frame, it is unable to shrink and tensile stresses develop. As the temperature drops further, the stress increases to a point when it reaches the specimen's tensile strength, and then fracture occurs. A typical load–temperature response from this type of test is shown in Figure 13.

The specimen sizes used by researchers varied—13 × 13 × 254 mm (Hills and Brien 1966), 25 × 25 × 305 mm (Monismith et al. 1965, Chipperfield and Fabb 1971, Fabb 1974, Sugawara et al. 1982, Sugawara and Moriyoshi 1984), 38 × 38 × 305 mm (Arand 1987), and 76 × 76 × 254 mm (Tuckett et al. 1970). The studies conducted by Chipperfield and Fabb, Fabb and Sugawara et al. used a liquid medium to lower the specimen temperature. All others used air as the cooling medium. The specimen sizes and cooling media used are summarized in Table 3.

The cooling rates reported in the literature ranged from 3 to 30°C/hr. Fabb (1974) and Sugawara et al. (1982) found that the fracture temperature and tensile strength were independent of cooling rate when it was equal to or greater than 5°C/hr; Sugawara et al. (1982) showed that tests at cooling rates less than 5°C/hr affected the fracture temperature (Fig. 14). For economy of time, most of the studies were conducted at cooling rates of 10°C/hr, even though these rates are higher than those found commonly in nature. Fromm and Phang (1971) reported that in Canada the cooling rate very

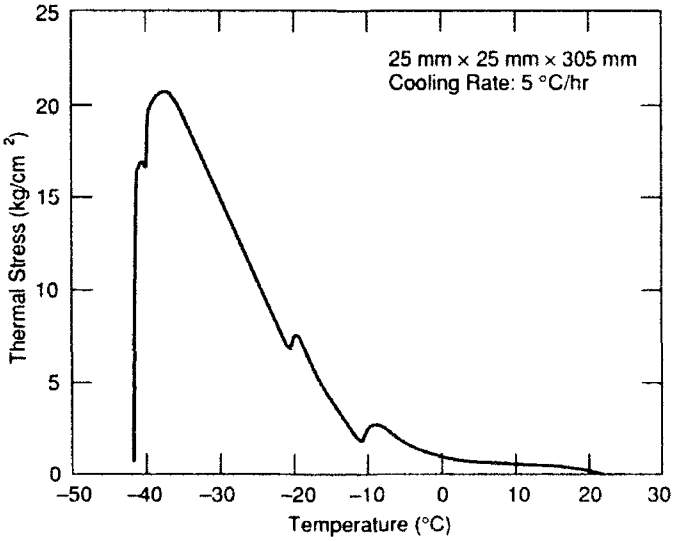

Figure 13. Typical stress–temperature curve.

Table 3. Summary of specimen sizes and cooling fluids used in thermal stress devices.

Investigators	*Specimen size (width × depth × length) (mm)*	*Cooling fluid*
Monismith et al. (1965)	25 × 25 × 305	Air
Hills and Brien (1966)	13 × 13 × 254	Air
Tuckett et al. (1970)	76 × 76 × 203	Air
Chipperfield and Fabb (1971)	25 × 25 × 305	50/50% water/antifreeze
Fabb (1974)	25 × 25 × 305	Methylated spirit
Arand (1987)	38 × 38 × 305	Air
Proposed SHRP	50 × 50 × 305	Air
Sugawara et al. (1982) and Sugawara and Moriyoshi (1984)	25 × 25 × 305	Methanol

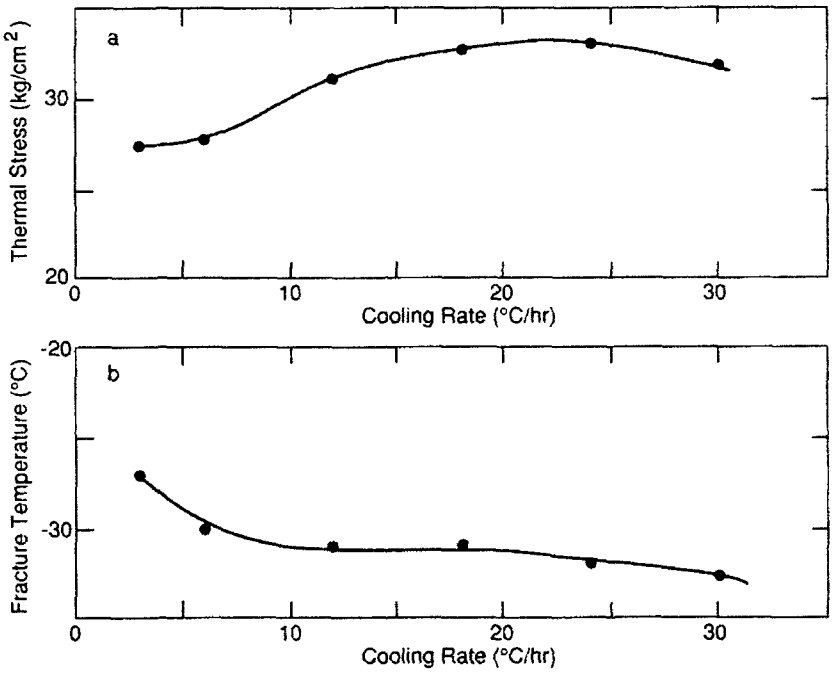

Figure 14. Effect of cooling rate on fracture strength and temperature (after Sugawara et al. 1982).

Table 4. Summary of cooling rates, crack observation and minimum temperatures reached in thermal stress devices.

Investigators	*Cooling rate used (°C/hr)*	*Crack observed*	*Minimum temperature (°C)*
Monismith et al. (1965)	?	No	0
Hills and Brien (1966)	10	Micro	Failure *
Tuckett et al. (1970)†	11	Yes	−9
Chipperfield and Fabb (1971)	10	No	−20
Fabb (1974)	5,**10****	Yes	Failure
Sugawara et al. (1982) and Sugawara and Moriyoshi (1984)	3,6,**12**,18,24 and **30**	Yes	Failure
Arand (1987)	10	Yes	Failure
Proposed SHRP	10	Yes	Failure

* The term failure is used to denote that the minimum temperature reached was sufficient to cause failure.

† The specimens were subjected to thermal cycling (−9 to 46°C/hr).

** Predominant cooling rate used in testing program.

seldom exceeds 3°C/hr. A summary of the cooling rates used, the minimum temperatures reached and observed cracks is presented in Table 4.

DEVELOPMENT OF THE CRREL THERMAL STRESS TEST (CTST)

The following criteria were used to develop the thermal stress device:

1. The test equipment should do thermal stress, thermal fatigue and creep compliance tests without requiring modifications.
2. The test system should provide accurate data on low-temperature cracking, thermal coefficient of contraction, creep compliance and thermal fatigue.
3. The cooling system should provide values of temperature drop and low temperatures likely to be seen in the field.
4. The monotonic and cyclic cooling rates should be controlled by a microprocessor.

System 1—steel–aluminum specimen loading system (SLS)

The development of the CTST started at CRREL before 1987, before the involvement of the present authors. We inherited the test equipment shown in Figure 15, which had three components: 1) the Specimen Loading System (SLS), 2) the environmental chamber and 3) the data acquisition system. The major components of the SLS system included a rigid A-36 grade steel frame that was 102 cm long × 48 cm wide × 33 cm high × 2.5 cm thick, and an aluminum tube. The test specimen was restrained between one end of the steel frame and the aluminum tube. On the other end of the aluminum tube, a temperature-compensated (between –18 and 66°C), 44-kN-capacity load cell was attached. This load cell was used to measure the tensile load in the sample from the applied thermal load. The back of the load cell was attached to the steel frame. The shrinkage of the stiffer steel frame was determined so as to be exactly compensated for by the shrinkage of the shorter aluminum tube during temperature cycling, thus restricting the AC test specimen's shrinkage and producing the required $\varepsilon_{axial} = 0$ condition.

Temperature was initially controlled using a box that was insulated by rigid foam and placed in a walk-in coldroom that could be cooled to –40°C. A heater and fan system was installed in the box for better temperature control. The fastest cooling rate possible with this setup was 2.5°C/hr, but we considered this inadequate because higher cooling rates were required for our study. We also found that the defrost cycle in the coldrooms was adversely affecting the temperature in the box. So, the insulated box in the coldroom scheme was abandoned. Later, a specially designed air cooling unit from another project became available. This unit was capable of producing temperatures in the range of –100 to 100°C. With an aid of a programmable temperature controller (OMEGA CN 2012-P2), the cooling unit was capable of producing cooling rates up to 27°C/hr. Other modifications included building a tighter, sturdier environmental chamber for housing the SLS. The resulting modified environmental chamber is shown in Figure 16.

The initial data acquisition–control system consisted of a hand-held HP 71B computer and an HP 3421A data acquisition system. The data were stored on flexible micro-disks and hard copies were printed on an HP ink jet printer. With time, the hand-held calculator was replaced with a personal computer, and the data acquisition system was upgraded. The temperature, load and deformation measurements were made through this

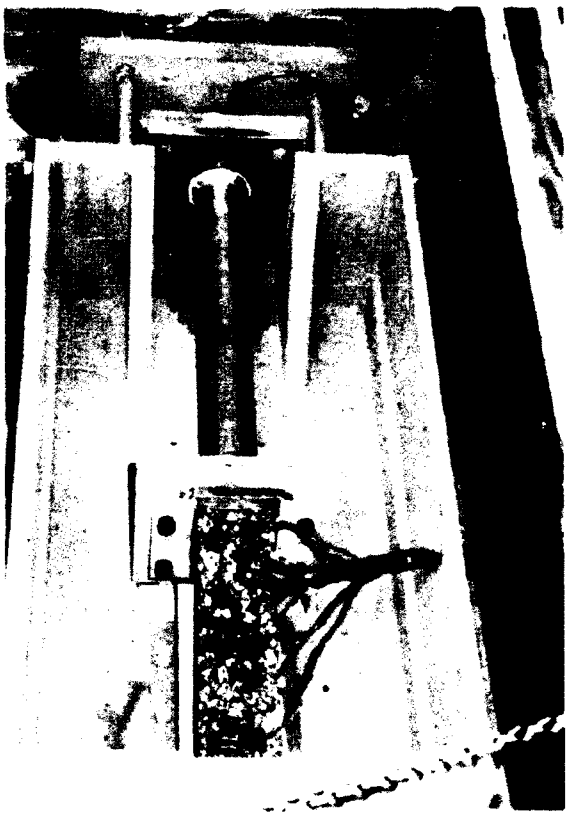

Figure 15. First CRREL thermal stress device (system 1).

Figure 16. Environment chamber and data acquisition system.

system. Although the design of the SLS was predicated on zero axial deformation, actual deformation of the AC test samples was monitored with four Linear Variable Differential Transformers (LVDTs), whose nominal linear range was ±2.5 mm. The data acquisition system is also shown in Figure 16.

The thermal stresses induced by temperature changes measured with this system were much lower than those reported by other investigators. A typical load–temperature response from this device is shown in Figure 17. As can be seen, the load was compressive instead of tensile. We think that the compressive load was caused by a net shortening of the restraining system holding the test sample. Fabb (1974) found that movements in excess of 0.025 mm produced tensile load errors greater than 20%. Therefore, it was important to minimize any movements in the AC during the test. We made several modifications to the system attempting to correct this problem; however, we had very little success. Nonetheless, the test equipment was useful for studying the temperature variation in AC as the specimen was cooled. Tests were also conducted with the SLS to measure the coefficient of thermal contraction of AC. The results from these tests will be presented in a later section.

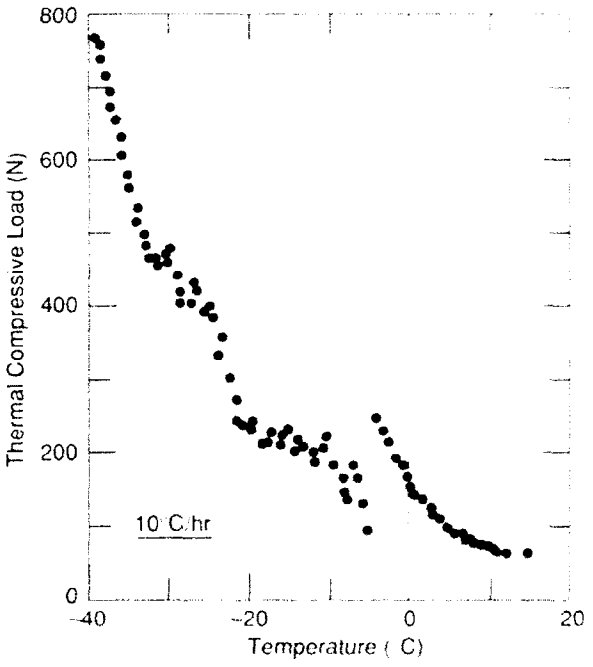

Figure 17. Thermal load response with temperature in system 1.

System 2—Invar rod system (IRS)

After more than a year's effort to correct the error from the SLS, another approach was taken. Rather than trying to fully compensate for differential thermal expansion and contraction of the specimen holder, we designed a second system that would minimize the effects of varying temperatures. The device consisted of a frame of four Invar-36 bars between two end plates, with a load cell and a specimen mounting plate in between (Fig. 18). Invar was chosen for this application because of its very low mean thermal coefficient of

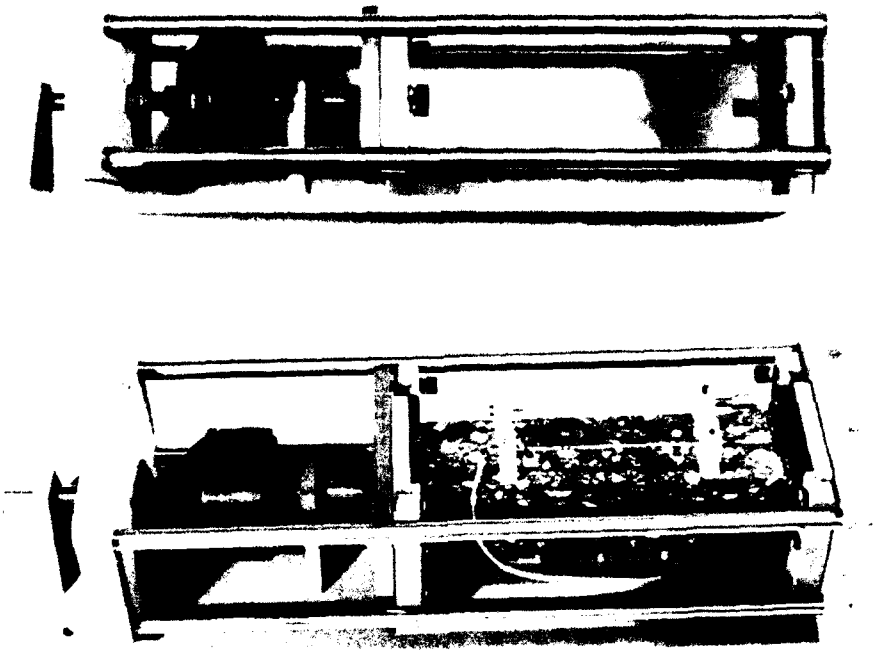

Figure 18. Invar Rod System (IRS), system 2.

expansion (9×10^{-7}/°C) and relatively high modulus of elasticity (148 GPa). The objective of this design was to provide a simple, stiff mounting frame that would not be adversely affected by varying ambient temperatures.

The specimen, as used in this fixture, is mounted in Invar end caps using epoxy adhesive. For testing, a mounted specimen is inserted in the fixture and attached to a fixed end plate and a mounting plate, which is attached to the floating end plate through the load cell. Stresses on the sample caused by thermally induced strains in the fixture were minimized by using Invar for most of the critical components in the fixture. Some steel was used to compensate for the Invar shrinkage, although this was not the basis of the design. The similar thermal conductivity and masses of the steel and Invar components ensured that the thermal responses of the different components would be comparable, thus reducing the stress–strain fluctuations that occurred with the previous SLS design.

Instrumentation for the Invar Rod System (IRS) was essentially the same as that used during the latter stages of testing with the original SLS. The 44-kN load cell was replaced with a 22-kN Kulite load cell, whose nominal deflection was 0.025 mm at 22 kN. No changes were made to the cooling system, and initial tests were run in the thermal chamber constructed for the SLS.

Initial tests in the IRS with 76- × 76-mm specimens were promising, resulting in higher, more even loads than with the original device. Tests with small specimens (25 × 25 mm) were especially encouraging. However, the frame did not prove to be stiff enough for the loads encountered with the larger specimens. A lack of corroborating data for large specimens led us to believe that some redesign of the fixture would be necessary. Larger, stiffer Invar rods (⌀ 25.4 mm) were used to replace the ⌀ 15.9-mm rods of the original design. The rods were also wrapped in insulating tape to retard heat transfer and more closely correlate the thermal response of the rods to that of the specimens. A nitrogen gas cooling system was also designed and incorporated into the IRS system to improve the portability of the system. Testing with this system is currently on hold owing to the development of a third system, which will be discussed next.

System 3—step motor system (SMS)

Although the IRS worked well with samples up to 50 × 50 mm, more consistent tests with the larger

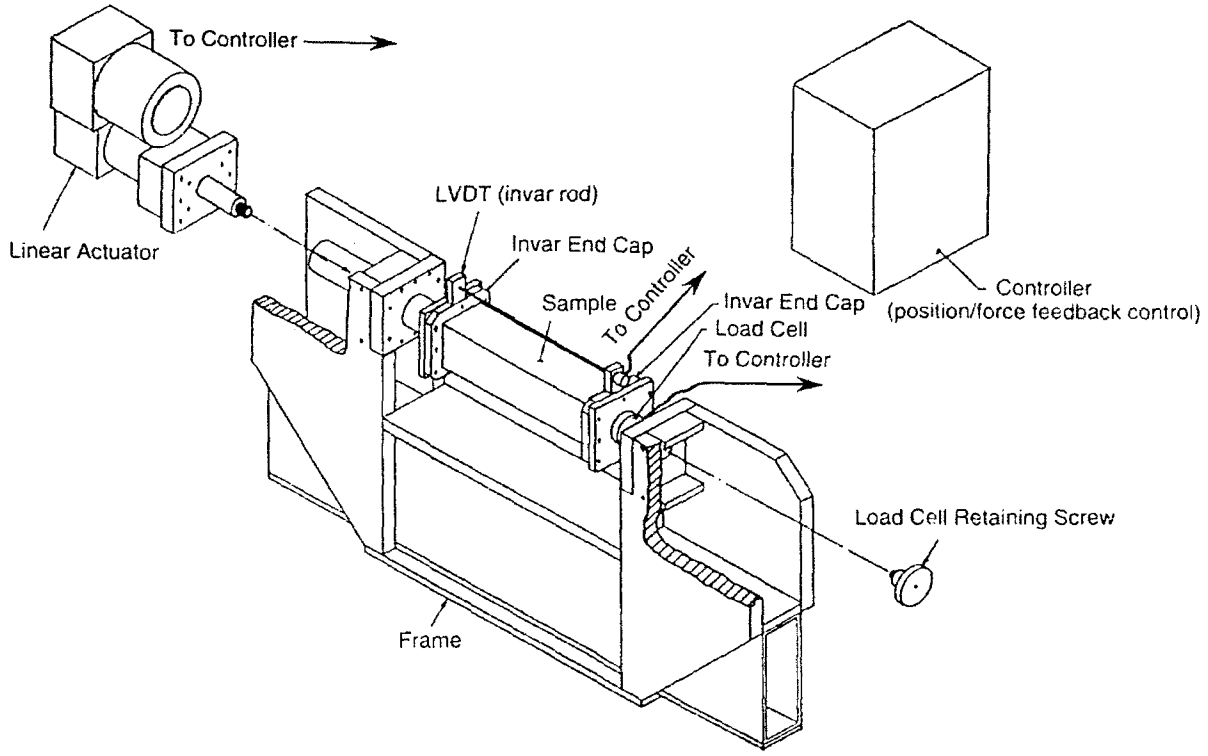

Figure 19. Step Motor System (SMS), system 3.

76- × 76-mm samples were desired. A massive specimen holder, with a rigid steel frame and a servo-controlled step motor, was the next step in the evolution of thermal stress test devices. This device, as designed, had the additional feature of partially isolating the thermal cycling environment from the holding device. A linear positioning device with closed-loop feedback was installed on the system, after initial tests, to more closely control the length of the specimen. Figure 19 illustrates the complete system minus the thermal cycling chamber. Figure 20 shows the load frame with a specimen mounted in the thermal chamber.

Originally, a load frame without the length-maintenance feedback system was envisioned. The frame was constructed to withstand forces of 9 kN

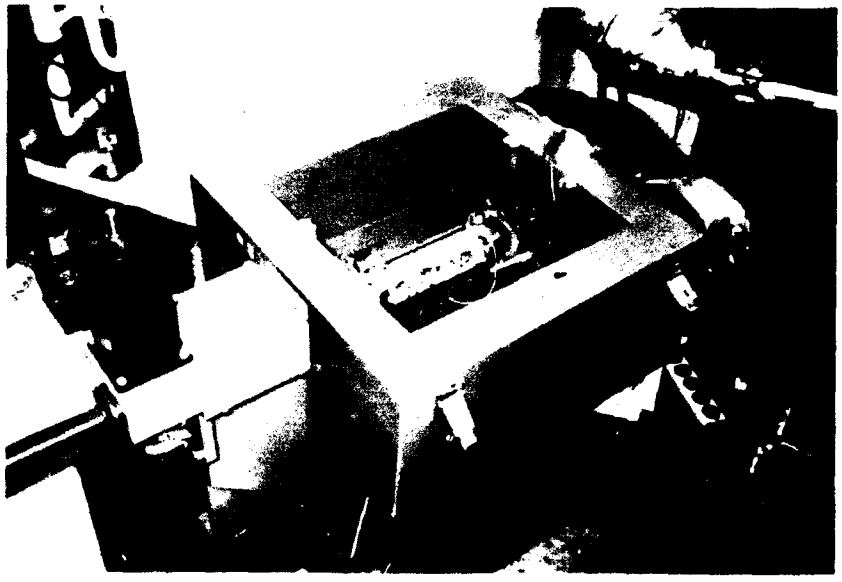

Figure 20. SMS with specimen in place.

with a deflection of less than 0.08 mm, but testing with an aluminum control sample indicated that deflections were greater than originally anticipated. Structural modifications to the frame increased stiffness to about 0.02 mm for a 9-kN load (0.05 mm at 22 kN) at room temperature. Further analysis of the system during thermal cycling tests indicated that there was greater heat transfer than anticipated between the thermal cycling chamber and the frame, resulting in distortion of the frame and partial unloading of the sample. Attempts to correct this problem with heat blankets proved impractical, so alternative active methods of compensating for the deformations in the frame were sought.

One of the original ideas discussed at CRREL for controlling the sample length over varying load–temperature conditions employed a servo-drive–ball-screw mechanism using feedback control. Because of the high costs of such a system then (1988) and the desire to use as much of the existing SLS (system 1) as possible, this option was not pursued. Correspondence with the Transportation Research Institute of the Oregon State University indicated that they had assembled a cost-effective system using a load frame similar to the CRREL model employing a Parker Compumotor servo motor and drive in conjunction with a Joyce/Dayton jackscrew. A similar combination of components was purchased and integrated into the existing load frame at CRREL. Figure 21 shows the motor–drive screw system.

The drive system consists of a Parker Compumotor Plus driver (64-CHP-DRIVE) and motor with resolver (64-CP106–220). The system is controlled by a personal computer running a Compumotor PC23 three-axis controller (64-PC23). The driver has step and direction input from the indexer, with closed-loop feedback from the motor resolver. Repeatability is ±0.00034, accuracy ±0.100° and resolution 25,600 steps per revolution. The motor has a continuous rated torque of 7.77 N m, with a rotor inertia of 9.28×10^{-3} N m^2. The indexer has a stepping accuracy of ±0.00 steps with a position range of 0 to 99,999,999 steps. The board is based on an IBM personal computer and was used in an Intel 286-based computer. It has the capability of six inputs and outputs, linear interpolation and encoder feedback (not used). All specifications are manufacturer-based.

The drive screw is a Joyce/Dayton Model AR-WJT242–24-INV-T 3 (keyed) 2-ton capacity jack screw. The screw pitch is 6.35 mm acme with a diameter of 25.4 mm. The screw is driven through a right-angle worm drive with a 24:1 ratio. The worm gear acts as a nut to drive the nonrotating acme screw. In addition, the worm gear is split to avoid backlash when reversing direction.

The LVDT instrumentation on the test sample interacts with the servo-drive, providing the feedback control necessary to maintain the sample length over varying parts of the test (Fig. 22). At startup, the sample is in place in the specimen holder, usually with a slight initial load to take up any slack. As the temperature in the enclosure falls, the sample attempts to shrink, resulting in a force in the sample-constraining structure (frame, jack screw, load cell, etc.). This force causes distor-

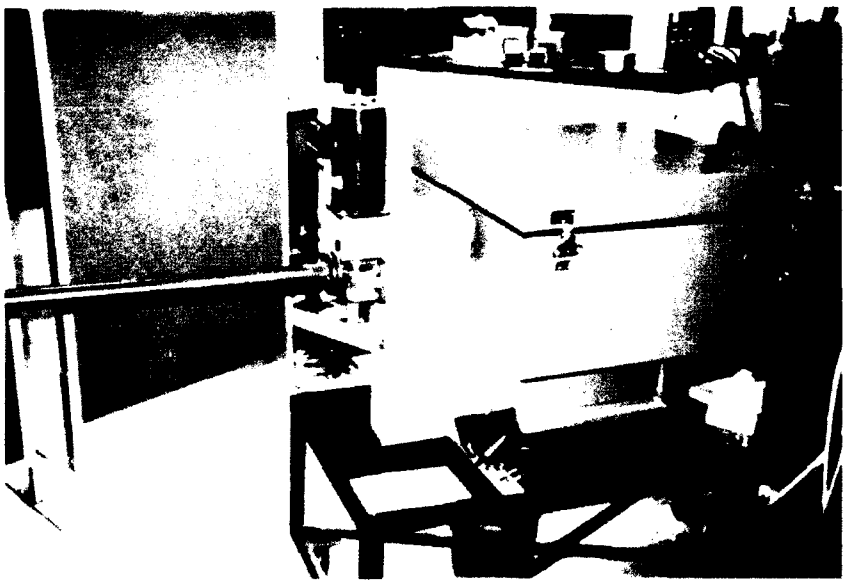

Figure 21. Motor–drive screw setup in SMS.

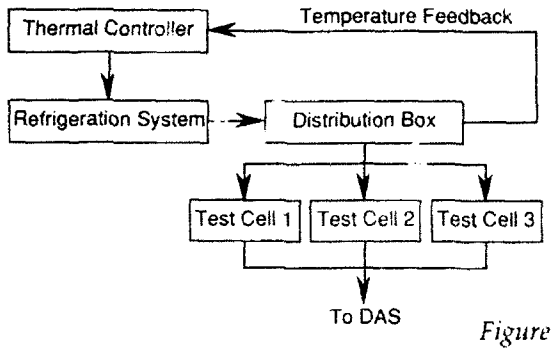

Figure 22. Feedback control system (DAS = data acquisition system).

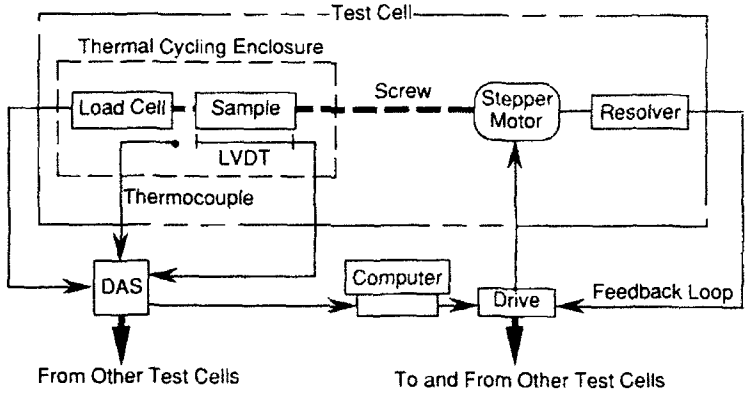

tion in the support structure that, if not compensated for, would allow the sample to shrink axially and thus partially unload. As the sample shortens, the length control LVDTs register a decrease in length by varying their output voltage. This analog output signal is compensated for ambient temperature (derived from a thermocouple near the LVDT) and is fed into the servo-drive for the stepper motor that positions the jack screw. A command to move a fixed number of pulses is sent to the stepper motor to correct for this length differential. A resolver, connected to the drive motor, returns to the driver the number of steps taken during the scan interval of the driver. Any difference between the two is considered error and the motor is commanded to make up the difference. This feedback control loop will maintain the sample length whether the sample is shrinking or expanding, thus compensating for both decreasing and increasing temperatures.

To minimize fracture induced by the stress concentration close to the end caps, swivel joints were added to hold the test specimen to the load cell and the screw jack, reducing noneccentric loading near the end of the samples. This joint was used for monotonic load tests and was replaced with a rigid joint for thermal cycling tests. In the cycling tests, during the warming cycle, the specimen tended to expand. The step motor then applies a compressive load on the specimen. With a swivel joint, this compressive load could not be applied uniformly.

EQUIPMENT CALIBRATION

Load cell

The load cell in the SMS is subjected to the same cooling as is the asphalt specimen. The load cell is a Kulite Semiconductor Products, Inc. (Model TC–2000–5000), 22-kN tension compression load cell that has a special low-temperature (–40°C) compensation. Nominal deflection at full load is 0.025 mm. It employs a stainless steel diaphragm and a four-arm Wheatstone semiconductor bridge, integrally compensated for temperature fluctuations.

Tests were conducted to study the influence of monotonic temperature loading on the output response of the load cell. The load cell, attached to the equipment, was set up free from any applied loads as the temperature was dropped 10°C/hr. Some additional tests were conducted with other temperature change rates. In addition, the influence of two starting temperatures was also studied: 20 and 10°C. The results from a regression analysis are presented in Figure 23. The load cell output indicated compression as the temperature

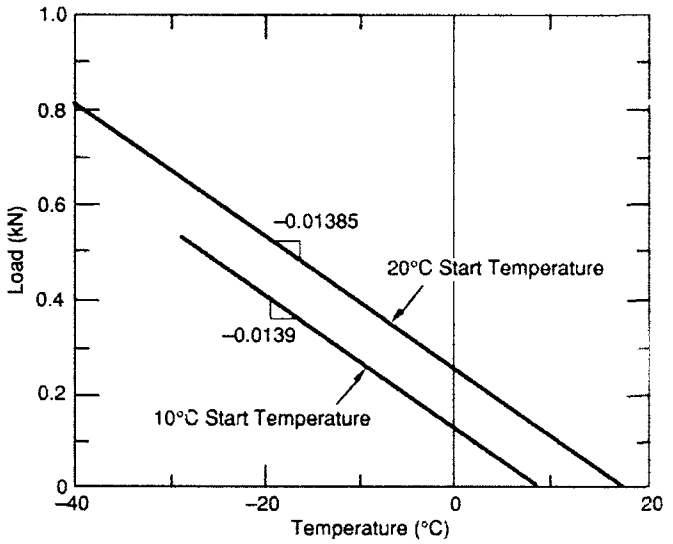

Figure 23. Load cell calibration for monotonic thermal loading.

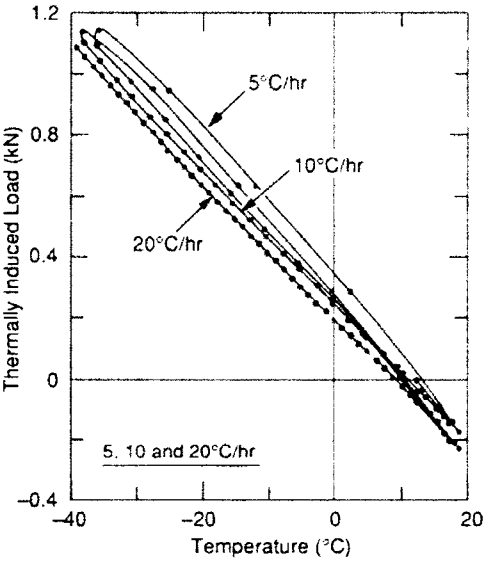

Figure 24. Hysteresis in the load–temperature curve seen during warming.

dropped. The initial value was a function of the starting temperature; however, the rate of change in the load with temperature was constant. The total tensile load can be written as a function of the form

$$\text{Load}_{(\text{total})} = \text{Load}_{(\text{AC})} + \text{Load}_{(\text{load cell})}$$

where $\text{Load}_{(\text{AC})}$ is the thermal load from the restrained AC specimen and $\text{Load}_{(\text{load cell})}$ is the load from the change in load cell temperature.

On the basis of regression analysis ($r^2 = 0.96$), the $\text{Load}_{(\text{load cell})}$ can be estimated from

$$\text{Load}_{(\text{load cell})}\ (\text{kN}) = \text{Initial Value} - 0.0139 \bullet \text{Temperature}\ (°\text{C}).$$

For cyclic thermal loading tests, the load cell is calibrated for the temperature range at which the test is to be conducted. Results from experiments conducted at 5, 10 and 20°C/hr showed a hysteresis in the load–temperature curve during warming (Fig. 24). Although this hysteresis is small, we decided to calibrate the load cell to specific temperature cycles. An example of a cyclic load calibration test is shown in Figure 25. In most of the thermal cycling tests, we were interested in the load at the minimum and maximum cycle temperatures. These values are corrected for the load cell variation with temperature. As shown in Figure 26, the variation in the load with temperature is fairly constant with repeating cycles. However, there were times when this was not so. Therefore, we decided to modify the test apparatus so that the load cell is outside the environmental box. The modification would connect the end plate to the outside load cell using a low-temperature conducting ceramic.

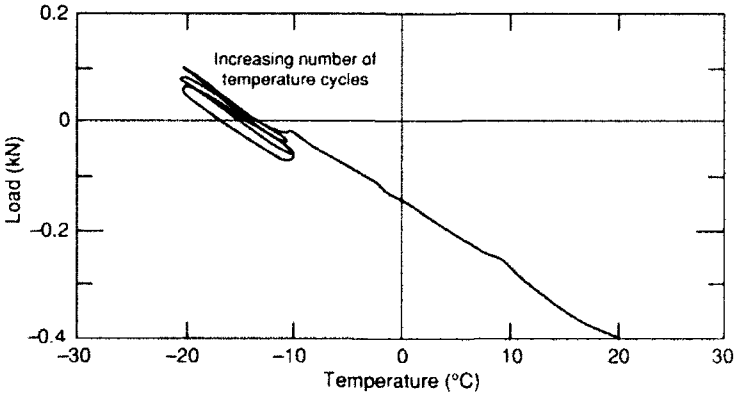

Figure 25. Influence of cyclic temperature on load cell measurements.

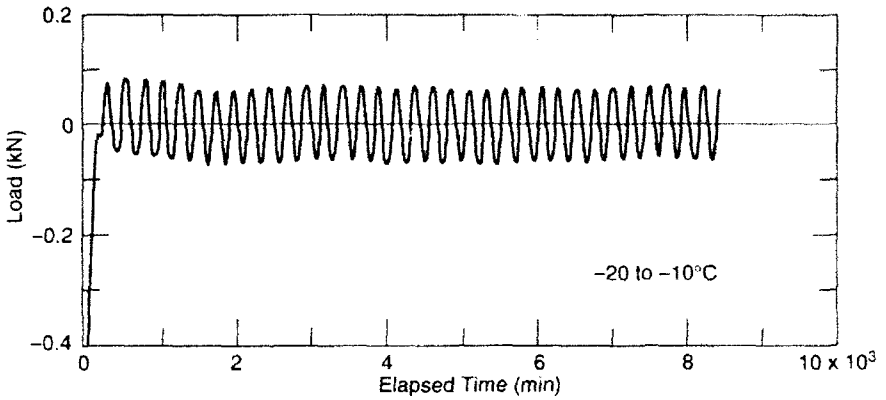

Figure 26. Change in load cell measurements with time.

Linear variable differential transformers (LVDTs)

As shown in Figure 27, the displacement measurement system consists of a stainless steel barrel and core, brass and invar extension rods and Plexiglas fixtures. All of these materials will contract when cooled, and affect the displacement measurement.

The LVDTs used were the Schaevitz miniature MHR series, with a nominal linear range of ±0.254 mm and operating range of –55 to 150°C. The sensitivity of the LVDTs was 0.254 mm/10 V.

The LVDTs were calibrated in the environmental chamber using a hollow aluminum tube with a wall thickness of 3.2 mm as a standard (Fig. 28). The cold air was allowed to circulate around the surface and inside the tube, producing uniform shrinkage of the tube. The LVDTs were calibrated between 20 and –50°C. The temperature drops used for the calibration were 5, 10 and 20°C/hr. On the basis of these measurements, the following corrections were applied to the deformation measurements. The total measured deformation (δ_{total}) was the deformation of the aluminum less the sum of the deformations due to the brass core and invar extension rod, i.e.

$$\delta_{total} = \delta_{aluminum} - \delta_{invar} + \delta_{brass}.$$

The following coefficients of expansion were assumed: for the Invar, $k = 1.6 \times 10^{-6}/°C$ and for brass, $k = 21 \times 10^{-6}/°C$. A typical corrected average temperature–shrinkage relationship from the calibration is shown in Figure 29. Also shown in Figure 29 is the theoretical deformation of aluminum with temperature. A coefficient of thermal

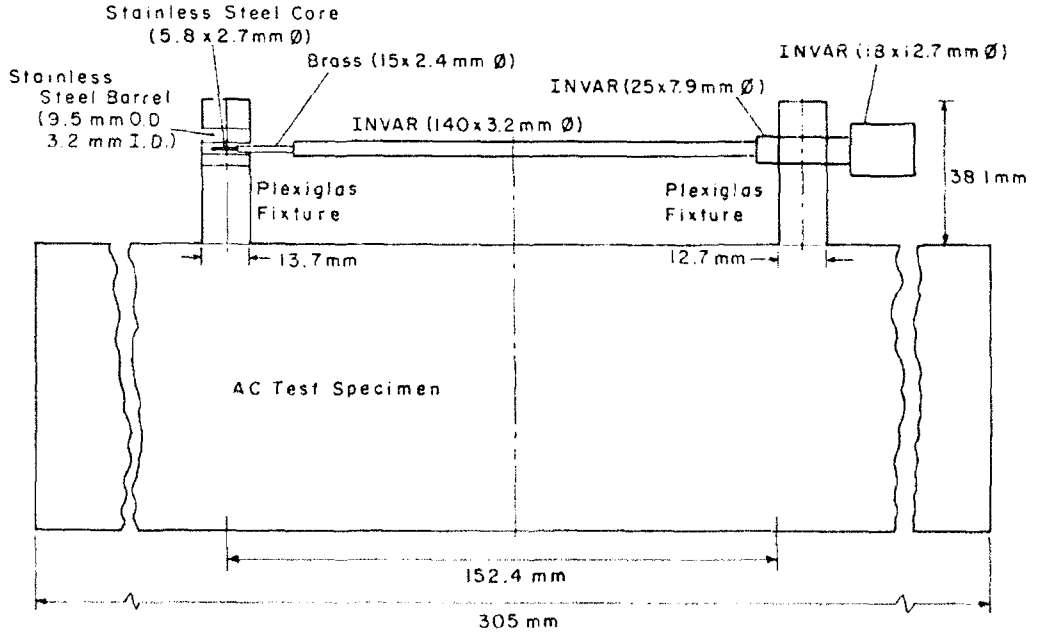

Figure 27. Displacement measurement system.

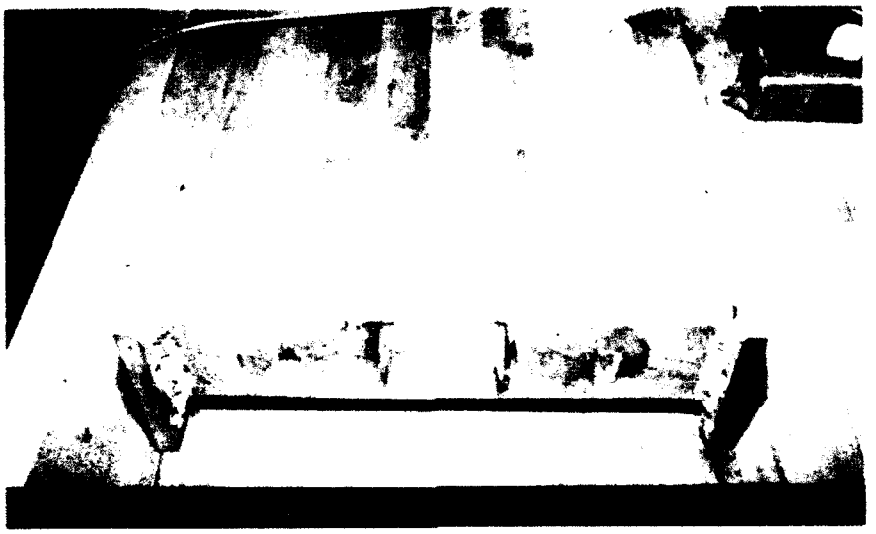

Figure 28. Hollow aluminum cylinder used to calibrate LVDTs and compliance of the various thermal stress devices.

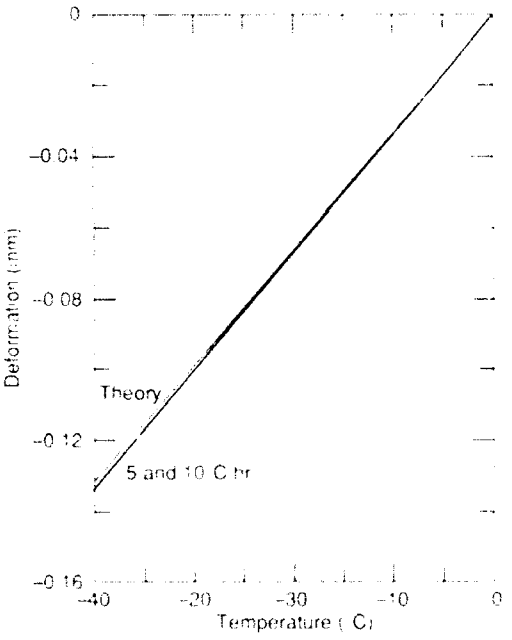

Figure 29. Typical corrected average shrinkage of aluminum.

expansion of $k = 21.4 \times 10^{-6}$/°C (Esbach 1985) was assumed for the aluminum. These coefficients were used to develop the displacement correction factor used for controlling the step motor in the SMS.

Temperature

The temperature distribution in a 76- × 76- × 305-mm specimen was also evaluated. Since the specimens were to be subjected to monotonic and cyclic thermal loading tests, we needed to know how quickly the temperature in an AC specimen reaches equilibrium, so several AC specimens were instrumented with Type T thermocouples at different locations (Fig. 30). The test specimens were then placed in the environmental chamber and subjected to 5, 10 and 20°C/hr cooling. Typical results are shown in Figure 31. As expected, the faster the rate of cooling is, the larger is the difference between the surface and the middle of the specimen. We experimented with different wait times at various temperatures and found that a 1-hour wait time was required for temperature equilibrium. On the basis of this finding, we established a 1-hour wait time standard between temperature drops. Also, for expediency, we settled for a cooling rate of 10°C/hr, although cooling rates as low as 3°C/hr can be generated with this test system.

DESCRIPTION OF TEST SPECIMENS

The specimens tested in these apparatuses had cross-sectional areas ranging from 25 × 25, 50 × 50, 76 × 25 to 76 × 76 mm. All had a length of 305 mm. These specimens can be made with a kneading compactor (ASTM D1561-81a) or, as in our case, the samples can be constructed in the field.

The field test sections were 10 m long × 3.7 m wide × 15.2 cm deep and were laid in two lifts in West Lebanon, New Hampshire. Different grades of asphalt were used in the mixture. Density measurements were made with the 4640 Troxler Nuclear Density Gage at several locations on the test sections. The minimum acceptable compaction density was 98% of the Marshall lab density (2.42 g/cm^3).

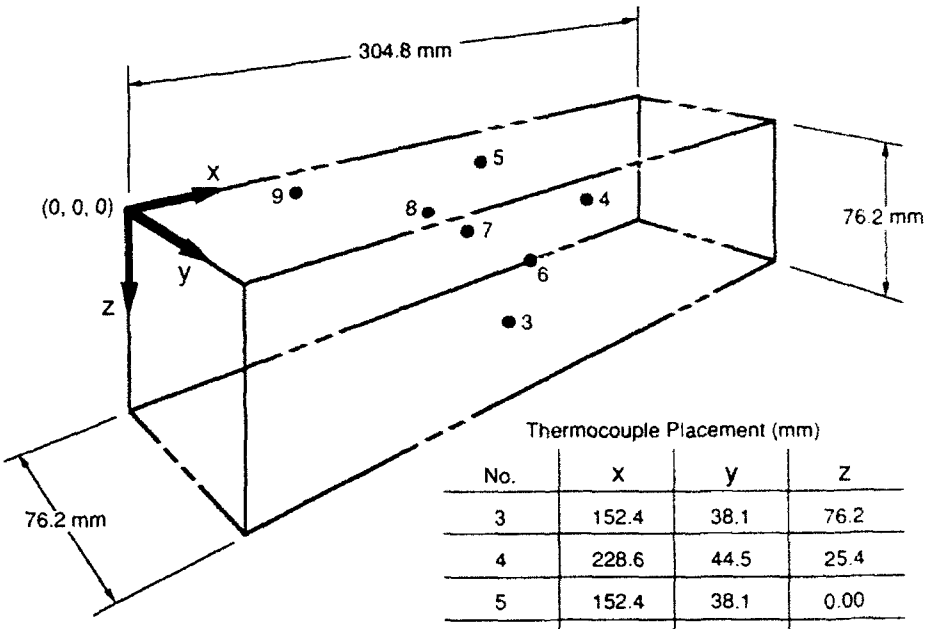

Thermocouple Placement (mm)

No.	x	y	z
3	152.4	38.1	76.2
4	228.6	44.5	25.4
5	152.4	38.1	0.00
6	165.1	38.1	50.8
7	152.4	38.1	38.1
8	139.7	38.1	19.1
9	76.2	12.7	12.7

Figure 30. Location of thermocouples within AC specimens.

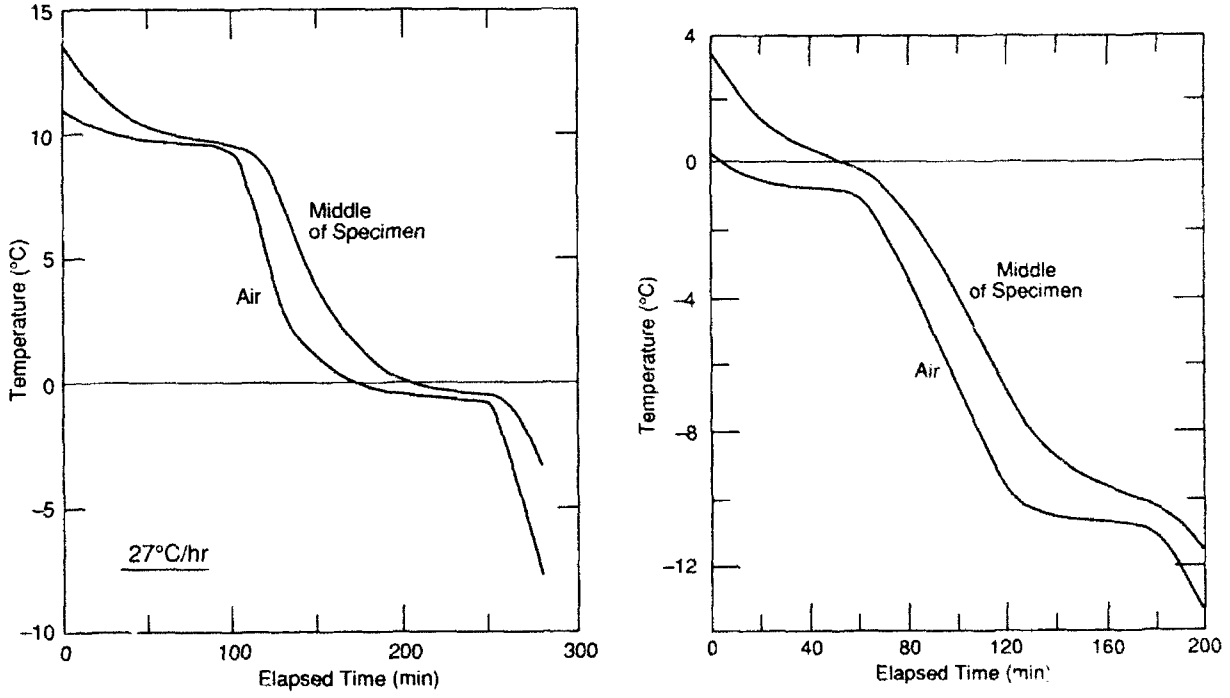

a. 27°C/hr cooling rate.

b. 10°C/hr cooling rate.

Figure 31. Variation of temperature in AC specimens.

To obtain test specimens, an area of 3.7 m long × 2.4 m wide was located within the test section (Fig. 32). Blocks of AC measuring 40.6 × 20.3 cm × 15.2 cm deep were cut from this area (Fig. 33). These blocks were shipped to CRREL, where they were further cut into the 305- × 76- × 76-mm test specimens. These specimens were cataloged and stored in a –7°C coldroom (Fig. 34). Typical test specimens of different cross sections are shown in Figure 35.

Our initial criterion for specimen size was a minimum cross section of 76- × 76-mm. Earlier studies concentrated on the 25- × 25-mm cross section. As seen in Figure 36, some of the aggregates are as large as the specimen width (or height), a situation that we considered to be inhomogenous because of the large aggregates. However, a study conducted with the IRS showed that, on the average, the change in the failure stress was small when specimen sizes were changed from 50- × 50-mm to 76- × 76-mm square (Fig. 37). On the basis of this finding, the Strategic Highway Research Program (SHRP) adopted a specimen size of 50 × 50 mm for the thermal stress test. CRREL has also adopted this size but continues to test 76× 76 mm whenever possible.

Figure 32. Test section from which samples were obtained.

Figure 33. Block samples from test section.

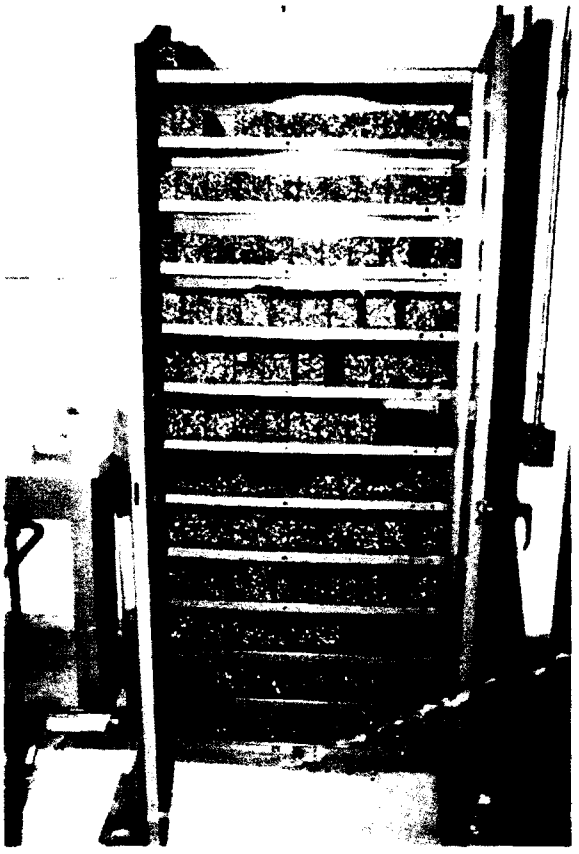

Figure 34. Specimens stored in coldroom.

TEST RESULTS

Some typical results are presented from tests conducted with the three systems for the SHRP program, for the Quebec Ministry of Transportation, and for in-house studies.

Coefficient of thermal contraction (*k*)

The coefficient of thermal contraction for AC was determined between a temperature range of 20 and –50°C. The tests were conducted in the SLS at cooling rates of 5, 10 and 20°C/hr.

For the tests, four LVDTs were attached to the test specimen using the jig shown in Figure 38. The jig was removed and the specimen was supported by two knife-edge stands in the environmental chamber. Deformation measurements were taken every 5 minutes. An average of all the deformation–temperature shrinkage tests conducted at 5°C/hr is shown in Figure 39. The slope of the deformation–temperature curve depends on temperature. This difference becomes more apparent at very low temperatures. The coefficient of thermal contraction (k) varies from 29×10^{-6} to 18×10^{-6}/°C as the temperature drops from 10 to –40°C. Similar values were found from tests conducted at 10 and 20°C/hr.

Thermal stress

Thermal stress tests were conducted in the IRS (system 2) and the SMS (system 3). We conducted the tests using monotonic and cyclic thermal loads in both systems on specimens of various cross sections. Typical load–temperature curves from the IRS are shown in Figure 40.

Most of the tests conducted with the IRS were on samples made in the field for CRREL. The asphalt in the mixture was specified to be an AC 10, and its PVN, based on CRREL test results, was –1.2. This, according to current Corps of Engineers specifications, is a high-temperature-susceptible asphalt. The AC mix, designed to meet the specifications for a Type III State of Vermont mix, had

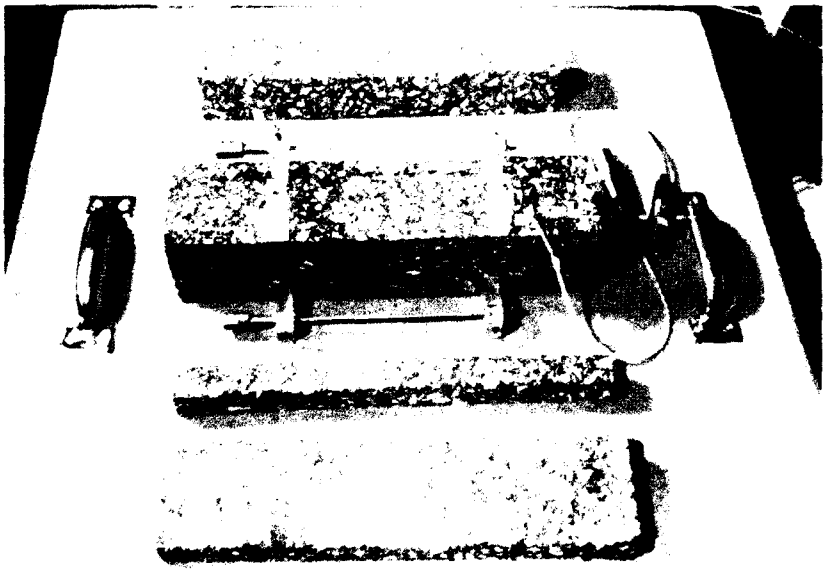

Figure 35. Different specimen cross sections used.

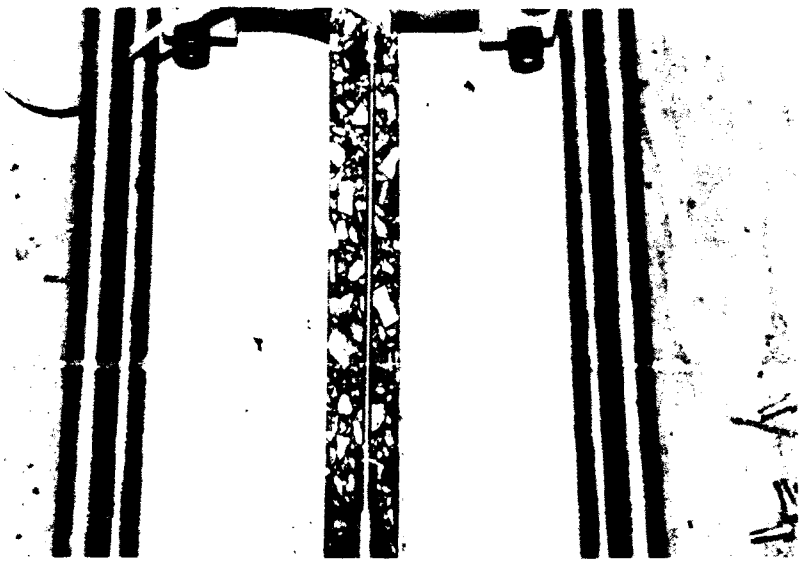

Figure 36. Specimen fracture in 25- × 25- × 305-mm sample.

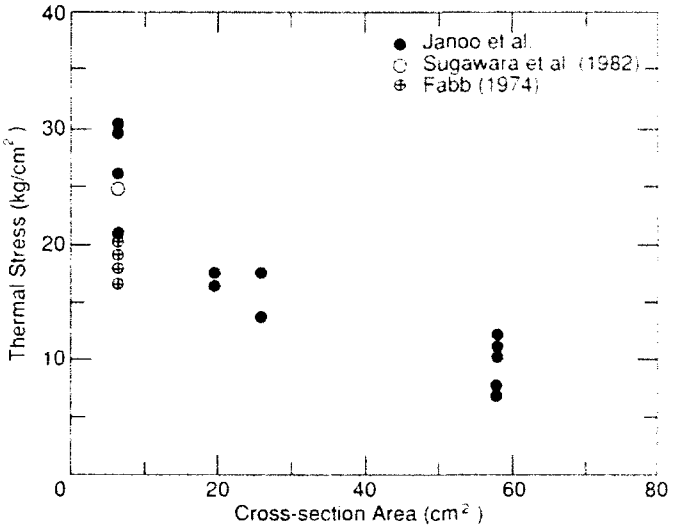

Figure 37. Effect of specimen cross-sectional area on thermal stress.

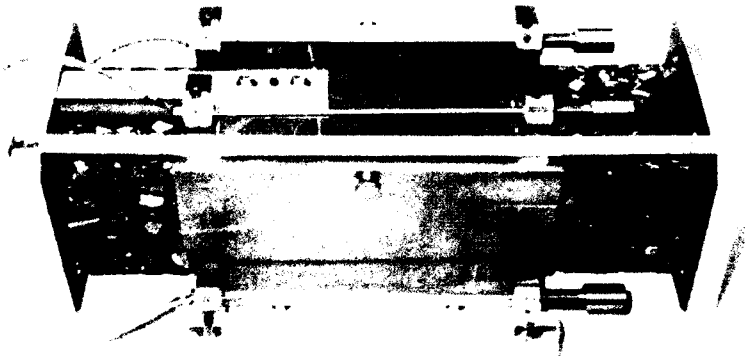

Figure 38. LVDT attachment jig.

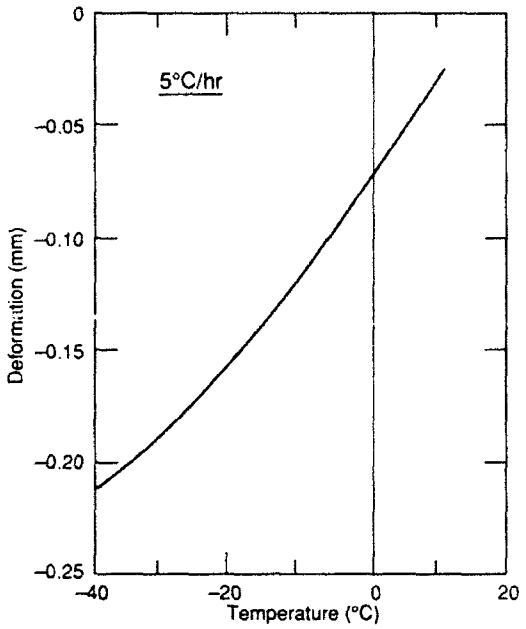

Figure 39. Typical results of deformation because of temperature changes in AC specimens.

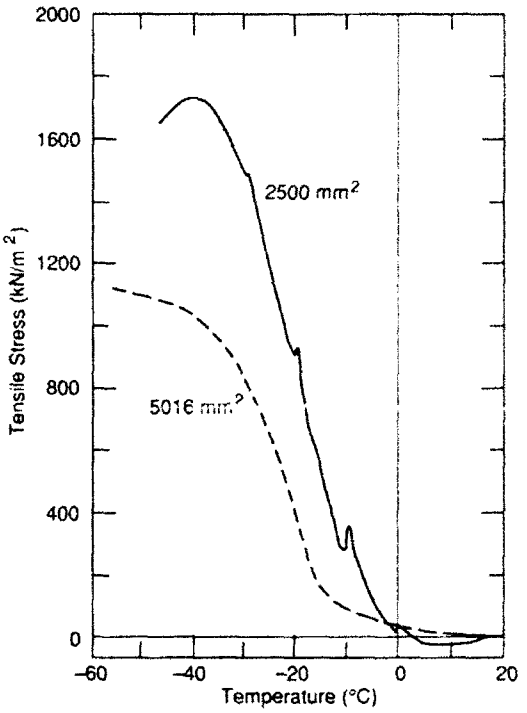

Figure 40. Typical thermal stress test results (IRS).

aggregates that were classified as not absorptive and a gradation that was similar to the low end of the Corps' surface course mix gradation. It also had an average air void of 4.36%, stability of 8674 N and a flow of 10.

In the IRS, the smaller 25- × 25-mm samples showed fracture at the end of the tests. For the 50- ×50-mm samples, the load drops off at low temperatures (Fig. 40). However, in many instances, the failure temperature (point where load drops) was lower than expected and there was no fracture. If a very small mechanical load is applied to the specimen at the end of the test, a fracture plane develops (Fig. 41). For the large 76- × 76-mm samples (Fig. 40), we often did not see the load drop at low temperatures or any failure planes at the end of the

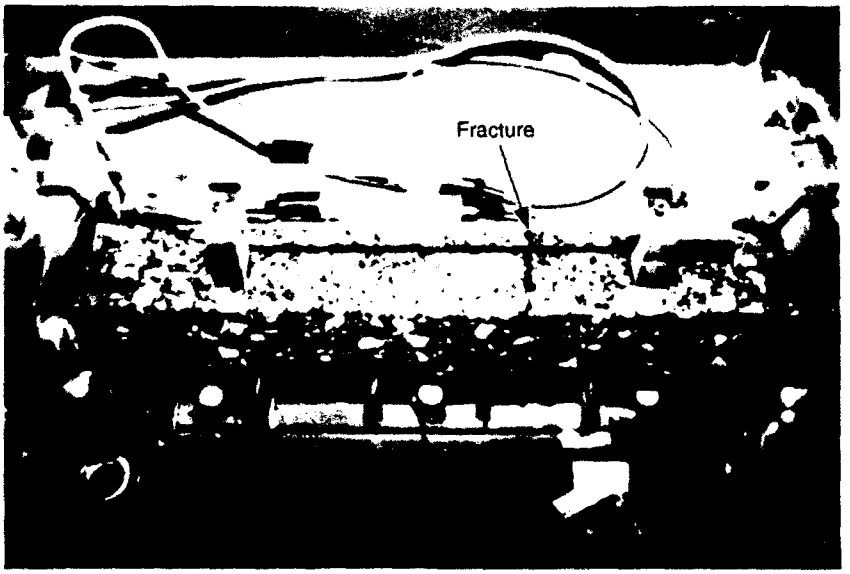

Figure 41. Fracture in specimen with 50- x 50-mm cross section.

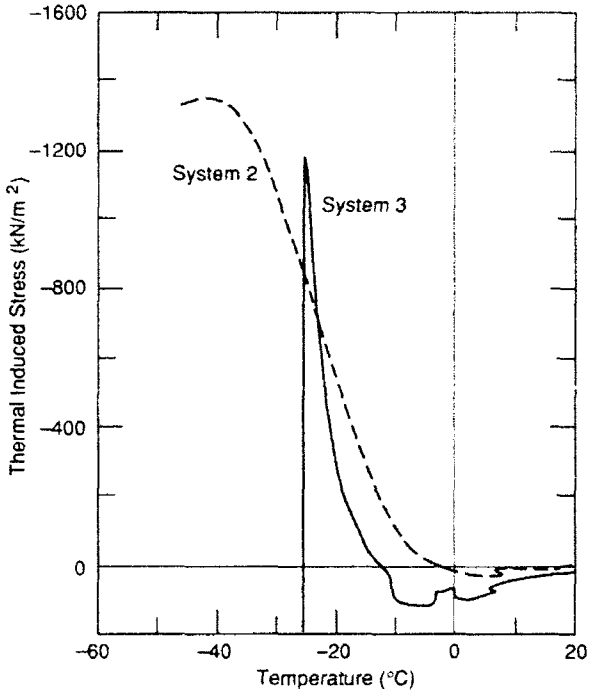

Figure 42. Comparison of failure temperatures from IRS (system 2) and SMS (system 3).

test because of the compliance of the system at low temperatures when large specimens are tested.

Two 50- × 50-mm test samples were tested simultaneously in the IRS and the SMS to examine the effect of compliance on the measured thermal loads. We found that, although the failure stresses were similar, the sample in the SMS failed at a higher temperature (–26 versus –40°C) (Fig. 42). The difference in the compliance of the two systems during thermal loading is shown in Figure 43. In the IRS, the movement is not controlled and the sample initially went into compression. The specimen began to shrink when the temperature fell below –10°C. The thick horizontal lines shown in the figure are the limits suggested by Fabb (1974). In the SMS, the sample also went into compression initially because the step motor was off. When the step motor was turned on at 10°C, it was able to control the expansion to the allowable level.

In this experiment, we attained better control of the deformation. Currently, in the SMS, the movement is controlled to ±0.01 mm. A photograph of the fracture plane in the samples tested in the SMS is shown in Figure 41. Also shown in Figure 41 is a "dog bone" AC test specimen. We are experimenting with this type of cross section to develop the failure planes away from the ends.

Thermal cycling tests were conducted for SHRP in the SMS. The 50- × 50-mm samples were prepared in the laboratory and provided to CRREL by SHRP. A typical cyclic temperature–load result for a specimen cycled between –10 and –20°C is presented in Figure 44. Results obtained by Sugawara et al. (1982) led us to initially assume that failure would take place after about 100 cycles. However, as the results show in Figure 45, there was a reduction in tensile thermal stress quite early in the cycling process that remained fairly constant after that. The reduction in thermal stress is the ratio of the current stress to the stress level prior to cycling. The thermal stress at –10°C drops to zero after approximately 70 cycles, indicating that the specimen has failed. The step motor actually applied a compressive load for a number of cycles to keep the sample from expanding. However, our visual inspection of the specimen at the end of the test showed no failure planes.

The hypothesis of thermal cracking caused by temperature cycling was not confirmed in our laboratory tests. As for the failures reported by Sugawara et al. (1982), we are not sure if the results were influenced by specimen size since they used a 25- × 25-mm specimen. Also, their temperatures were very close to monotonic failure temperatures. Further research in this area is needed.

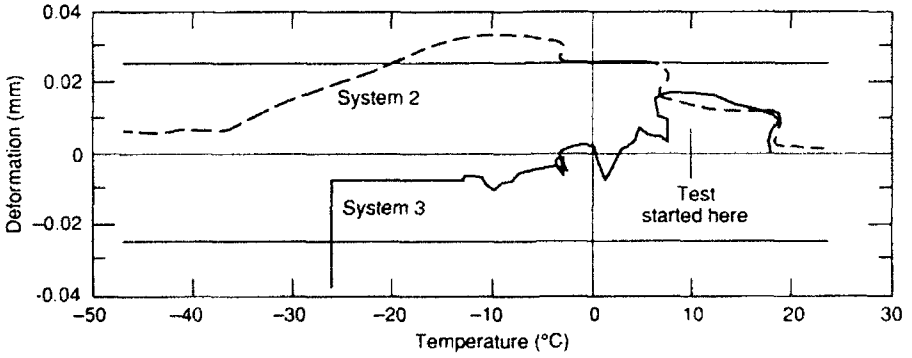

Figure 43. Variation in displacement in AC samples as measured in IRS (system 2) and SMS (system 3).

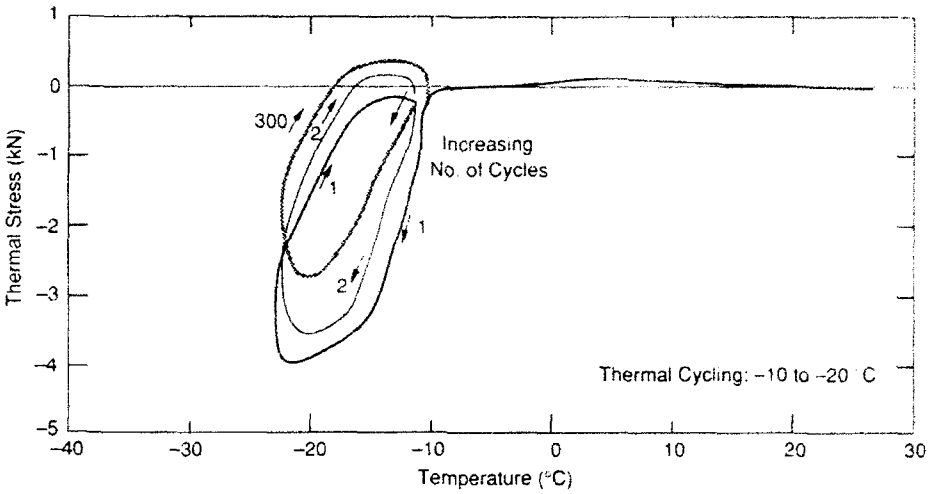

Figure 44. Typical cyclic test result.

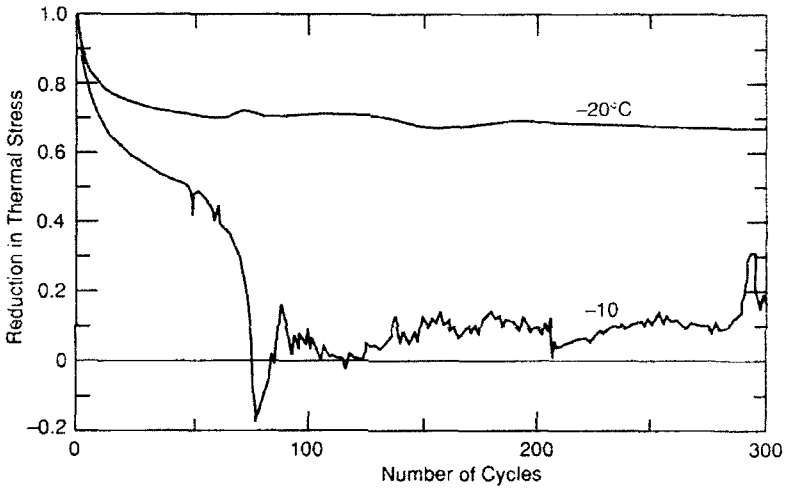

Figure 45. Reduction in strength because of temperature cycling.

SUMMARY

This report shows the various ways one can characterize AC performance at low temperatures. Basically, the characterization can be broken into direct or indirect measurements. The direct method is preferred, since the tensile load from thermal loading is measured directly. In the indirect method, the thermal stress is estimated based on some assumptions of the properties of the AC mixture.

A thermal stress device that employs a step motor and screw jack has been developed at CRREL for studying the reaction of *any* AC mixture to low temperatures and thermal fatigue. This device measures tensile load directly and appears to provide more realistic results than the other systems. Both monotonic and cyclic thermal loads can be applied to the specimen. The cooling system associated with this device is capable of generating cooling rates between 3 and 27°C/hr, and a minimum temperature of –60°C can be achieved. The device is capable of restraining movements in the test specimen to 25×10^{-5} mm. Various tests have been conducted with this apparatus and some of the results have been presented in this report.

This device will be used to develop criteria for AC pavements subjected to thermal stresses. The current Corps asphalt selection criteria for low-temperature performance and the SHRP criteria for performance of asphalt mixtures at low temperatures will be validated. Tests will also be conducted to study the performance of modified asphalt mixtures at low temperatures. Our goal is to find asphalt mixtures that will resist low-temperature cracking.

LITERATURE CITED

Ad Hoc Committee of the Asphalt Institute (1981) Design techniques to minimize low temperature asphalt pavement transverse cracking. The Asphalt Institute, Research Report No. 81–1.

Anderson, K.O. and S.C. Leung (1987) Applications of a method for evaluation of low-temperature tensile properties of asphalt concrete. In *Proceedings, Paving in Cold Areas Mini-Workshop*, vol. 1, p. 333–336.

Anderson, K.O. and W.P. Hahn (1968) Design and evaluation of asphalt concrete with respect to thermal cracking. *Proceedings of the Association of Asphalt Paving Technologists*, **37**: 1–31.

Anderson, K.O. and J.A. Epps (1983) Asphalt concrete factors related to pavement cracking in West Texas. *Proceedings of the Association of Asphalt Paving Technologists*, **52**: 151–197.

Arand, W. (1987) Influence of bitumen hardness on the fatigue behavior of asphalt pavements of different thickness due to bearing capacity of subbase, traffic loading and temperature. In *Proceedings of the 6th International Conference on Structural Behavior of Asphalt Pavements, University of Michigan*, vol. 1, p. 65–71.

Bonnaure, F., G. Gest, A. Gravois and P. Uge (1977) A new method of predicting the stiffness of asphalt paving mixtures. *Proceedings of the Association of Asphalt Paving Technologists*, **46**: 64–104.

Burgess, R.A., O. Kopvillem and F.D. Young (1971) St. Anne test road—relationships between predicted fracture temperatures and low temperature field performance. *Proceedings of the Association of Asphalt Paving Technologists*, **40**: 148–193.

Busby, E.O. and L.F. Rader (1972) Flexural stiffness properties of asphalt concrete at low temperatures. *Proceedings of the Association of Asphalt Paving Technologists*, **41**: 163–187.

Carpenter, S.H. and T. VanDam (1985) Evaluation of low-temperature performance of asphalt cements. Final Report submitted to USA Cold Regions Research and Engineering Laboratory, March.

Chipperfield, E.H. and T.R.J. Fabb (1971) Development of more durable road surfacing. In *Proceedings, Canadian Technical Asphalt Association*, vol. 16, p. 148–193.

Christianson, R.H.A. (1970) Analysis of the tensile splitting testing for low-temperature tensile properties of asphalt concrete. M.Sc. Thesis, The University of Alberta (unpublished).

Christison, J.T, D.W. Murray and K.O. Anderson (1972) Stress prediction and low-temperature fracture susceptibility of asphaltic concrete pavements. *Proceedings of the Association of Asphalt Paving Technologists*, **41**: 494–523.

Christison, J.T. (1966) The tensile splitting test applied to thermal cracking of asphalt pavements. M.Sc. Thesis, The University of Alberta (unpublished).

Deme, I.J. and F.D. Young (1987) Ste. Anne test road revisited twenty years later. In *Proceedings, Canadian Technical Asphalt Association*, vol. 32.

Dempsey, B.J., J. Ingersoll, T.C. Johnson and M.Y. Shahin (1980) Asphalt concrete in cold regions: A comparative laboratory study and analysis of mixtures containing soft and hard grades of asphalt cement. USA Cold Regions Research and Engineering Laboratory, CRREL Report 80–5.

Eshbach, O. (1985) *Handbook of Engineering Fundamentals*. New York: Wiley Handbook Series, 3rd edition.

Fabb, T.R.J. (1974) The influence of mix composition, binder properties and cooling rates on asphalt cracking at low temperatures. *Proceedings of the Association of Asphalt Paving Technologists*, **43**: 285–331

Finn F., C.L. Saraf, R. Kulkarni, K. Nair, W. Smith and A. Abdullah (1986) Development of pavement structural subsystems. National Cooperative Highway Research Program Report 291.

Finn, F.N., K. Nair and J. Hilliard (1976) Minimizing premature cracking of asphalt concrete pavements. *Proceedings of the Association of Asphalt Paving Technologists*, **45**: 492–529.

Fromm, H.J. and W.A. Phang (1971) Temperature susceptibility control in asphalt cement specifications. *Highway Research Record*, no. 350.

Fromm, H.J. and W.A. Phang (1972) A study of transverse cracking of bituminous pavements. *Proceedings of the Association of Asphalt Paving Technologists*, **41**: 383–423.

Gaw, W.J. (1978) The measurement and prediction of asphalt stiffness at low and intermediate pavement service temperatures. *Proceedings of the Association of Asphalt Paving Technologists*, **47**: 457–494.

Gaw W.J., R.A. Burgess and F.D. Young (1974) Ste. Anne test road: Road performance after five years and laboratory predictions of low temperature performance. *Proceedings, Canadian Technical Asphalt Association*, **XIX**: 45–98.

Haas, R.C.G. (1973) A method for designing asphalt pavements to minimize low-temperature shrinkage cracking. Asphalt Institute, Report 73–1.

Haas, R.C.G. and K.O. Anderson (1969) A design subsystem for the response of flexible pavements at low temperature. *Proceedings of the Association of Asphalt Paving Technologists*, **38**: 179–223.

Hass, R., H. Lee, F. Meyer and G. Argue (1987) Cold

climate performance of Canadian airport pavements. In *Proceedings of Mini Workshop 3, Paving in Cold Areas, July 20–22, Ottawa, Ontario*, vol. 1, p. 303–332.

Hadipour, K. and K.O. Anderson (1988) An evaluation of permanent deformation and low temperature characteristics of some recycled asphalt concrete mixtures. *Proceedings of the Association of Asphalt Paving Technologists*, **57**: 615–645.

Heukelom, W. and A.J.G. Klomp (1964) Road design and dynamic loading. In *Proceedings of the Association of Asphalt Paving Technologists*, **33**: 92–125.

Hills, J.F. and D. Brien (1966) The fracture of bitumens and asphalt mixes by temperature-induced stresses. Discussion. *Proceedings of the Association of Asphalt Paving Technologists*, **35**: 293–309.

Humphreys, J.S. and C.J. Martin (1963) Determination of transient thermal stresses in a slab with temperature-dependent viscoelastic properties. *Transactions of the Society of Rheology*, vol. VII

Janoo, V.C. (1990) Use of soft grade asphalts in airfields and highway pavements in cold regions. USA Cold Regions Research and Engineering Laboratory, Special Report 90–12.

Janoo, V.C. and E.J. Chamberlain (1987) Laboratory investigations of low-temperature cracking susceptibility of asphalt concrete. In *Proceedings of 3rd Workshop on Paving in Cold Areas, July 20–22, Ottawa, Ontario, Canada*, p. 397–416.

Janoo, V.C., T.S. Vinson, R. Hass and J. Bayer Jr. (1990) Test methods to characterize low-temperature cracking. In *Proceedings, 4th Workshop on Paving in Cold Areas, September 4–6, Sapporo, Hokkaido, Japan*, p. 255–288.

Jones, G.M., M.I. Darter and G. Littlefield (1968) Thermal expansion and contraction of asphaltic concrete. *Proceedings of the Association of Asphalt Paving Technologists*, **37**: 56–100.

Kallas, B.F. (1982) Low-temperature mechanical properties of asphalt concrete. The Asphalt Institute, Research Report 82–3.

Kennedy, T.W. (1977) Characterization of asphalt pavement materials using the indirect tensile test. *Proceedings of the Association of Asphalt Paving Technologists*, **46**: 132–150.

Linde, S. (1988) Investigations on the cracking behavior of joints in airfields and roads. Swedish National Testing Institute, Report 1988:23.

Littlefield, G. (1967) Thermal expansion and contraction characteristics of Utah asphaltic concretes. *Proceedings of the Association of Asphalt Paving Technologists*, **36**: 673–702.

McLeod, N.W. (1970) *Influence of Hardness of Asphalt Cement on Low-Temperature Transverse Pavement Cracking*. Montreal: Canadian Good Roads Association.

Monismith, C.L., C..A. Secor and K.R. Secor (1965) Temperature-induced stresses and deformation in asphalt concrete. *Proceedings of the Association of Asphalt Paving Technologists*, **34**: 248–285.

Osterkamp, T.E., G.C. Baker, B.T. Hamer, J.P. Gosink, J.K. Peterson and V. Groul (1986) Low-temperature transverse cracks in asphalt pavements in interior Alaska. Anchorage: Alaska Department of Transportation and Public Facilities, Report No. AK-RD–86–26.

Rader, L.F. (1935) Investigation of the physical properties of asphalt paving mixtures at low temperatures. In *Proceedings of the American Society for Testing and Materials*, Part II. vol. 35.

Rader, L.F. (1937) Report on further research work on correlation of low temperature tests with resistance to cracking of sheet asphalt pavements. *Proceedings of the Association of Asphalt Paving Technologists*.

Readshaw, E.E. (1972) Asphalt specifications in British Columbia for low-temperature performance. *Proceedings of the Association of Asphalt Paving Technologists*, **41**: 562–581.

Sato, K., T. Fukute and Y. Hachiya (1982) Thermally induced cracking due to hardening of asphalt concretes in airport asphalt pavements. In *Proceedings, Paving in Cold Regions Mini-Workshop*, vol. 1, p. 99–126.

Shahin, M.Y. and B.F. McCullough (1972) Prediction of low-temperature and thermal fatigue cracking in flexible pavements. Texas Transportation Institute, Research Report 123–14.

Shields, B.P. (1964) Current studies on transverse cracking of asphalt pavements. *Conference on Recent Developments in the Design and Construction of Asphalt Pavements, February, University of Alberta.*

Shields, B.P., K.O. Anderson and J.M. Dacyszyn (1970) An investigation of low-temperature cracking of flexible pavements. In *Proceedings, Canadian Good Roads Association.*

Sugawara, T. and A. Moriyoshi (1984) Thermal fracture of bituminous mixtures. In *Proceedings, Paving in Cold Areas Mini-Workshop*, vol. 1, p. 291–320.

Sugawara, T., H. Kubo and A. Moriyoshi (1982) Low-temperature cracking of asphalt pavements. In *Proceedings, Paving in Cold Areas Mini-Workshop*, vol. 1, p. 4–42.

Tuckett, G.M., G.M. Jones and G. Littlefield (1970) The effects of mixture variables on thermally-induced stresses in asphaltic concrete. *Proceedings of the Association of Asphalt Paving Technologists*, **39**: 703–744.

Van der Poel, C. (1954) A general system describing the viscoelastic properties of bitumens and its relation to routine test data. *Journal of Applied Chemistry*, **4**: 221.

Von Quintus, H.L., J.A. Scherocman, C.C. Hughes and T.W. Kennedy (1988) Development of asphalt aggregate mixture analysis system: AAMAS. Phase II. Preliminary Draft of Final Report .

REPORT DOCUMENTATION PAGE

Form Approved
OMB No. 0704-0188

Public reporting burden for this collection of information is estimated to average 1 hour per response, including the time for reviewing instructions, searching existing data sources, gathering and maintaining the data needed, and completing and reviewing the collection of information. Send comments regarding this burden estimate or any other aspect of this collection of information, including suggestion for reducing this burden, to Washington Headquarters Services, Directorate for Information Operations and Reports, 1215 Jefferson Davis Highway, Suite 1204, Arlington, VA 22202-4302, and to the Office of Management and Budget, Paperwork Reduction Project (0704-0188), Washington, DC 20503.

1. AGENCY USE ONLY (Leave blank)	2. REPORT DATE	3. REPORT TYPE AND DATES COVERED
	July 1993	

4. TITLE AND SUBTITLE

Thermal Stress Measurements in Asphalt Concrete

5. FUNDING NUMBERS

DTFA01-89-Z-02050

6. AUTHORS

Vincent Janoo, John Bayer, Jr. and Michael Walsh

7. PERFORMING ORGANIZATION NAME(S) AND ADDRESS(ES)

U.S. Army Cold Regions Research and Engineering Laboratory
72 Lyme Road
Hanover, New Hampshire 03755-1290

8. PERFORMING ORGANIZATION REPORT NUMBER

CRREL Report 93-10

9. SPONSORING/MONITORING AGENCY NAME(S) AND ADDRESS(ES)

U.S. Department of Transportation
Federal Aviation Administration
Research and Development Service
Washington, D.C. 20591

U.S. Army
Office of the Chief of Engineers
Washington, D.C. 20314-1000

10. SPONSORING/MONITORING AGENCY REPORT NUMBER

DOT/FAA/RD/92/13

11. SUPPLEMENTARY NOTES

12a. DISTRIBUTION/AVAILABILITY STATEMENT

Approved for public release; distribution is unlimited.

Available from NTIS, Springfield, Virginia 22161.

12b. DISTRIBUTION CODE

13. ABSTRACT (*Maximum 200 words*)

Asphalt concrete (AC) pavements in cold regions are prone to thermal cracking. There are two theories to explain this. The first one is that at some low temperature, the thermal stress in the pavement structure exceeds the tensile strength of the mixture, usually in the winter. The second is that the AC mixture fails through thermal fatigue that is caused by daily temperature cycling. There are many ways of characterizing AC performance at low temperatures, and this report summarizes the different failure criteria and test methods for doing this. One test method described here that CRREL has developed is a thermal stress test device for measuring thermally induced stresses in the laboratory. The device can be used for monotonic and cyclic loading, while various temperature drop rates can be applied to the specimen. The calibration of the test apparatus, loading pattern and specimen configuration used are described and typical results are presented.

14. SUBJECT TERMS

Asphalt concrete
Cracking
Cold regions
Flexible pavements
Thermal cracking
Thermal stress
Thermal stress test

15. NUMBER OF PAGES
38

16. PRICE CODE

17. SECURITY CLASSIFICATION OF REPORT	18. SECURITY CLASSIFICATION OF THIS PAGE	19. SECURITY CLASSIFICATION OF ABSTRACT	20. LIMITATION OF ABSTRACT
UNCLASSIFIED	UNCLASSIFIED	UNCLASSIFIED	UL